Mon. Not. R. Astron. Soc. **000**, 1–21 (2010) Printed 13 April 2010 (MN LATEX style file v2.2)

# A semi-analytic model comparison - gas cooling and galaxy mergers

Gabriella De Lucia[1⋆], Michael Boylan-Kolchin[2], Andrew J. Benson[3], Fabio Fontanot[1], Pierluigi Monaco[1,4]
[1] *INAF - Astronomical Observatory of Trieste, via G.B. Tiepolo 11, I-34143 Trieste, Italy*
[2] *Max–Planck–Institut für Astrophysik, Karl–Schwarzschild–Str. 1, D-85748 Garching, Germany*
[3] *MC350-17, California Institute of Technology, Pasadena, CA 91125, USA*
[4] *Dipartimento di Astronomia, Università di Trieste, via G.B. Tiepolo 11, I-34131 Trieste,Italy*



13 April 2010

**ABSTRACT**
We use stripped-down versions of three semi-analytic galaxy formation models to study the influence of different assumptions about gas cooling and galaxy mergers. By running the three models on identical sets of merger trees extracted from high-resolution cosmological $N$-body simulations, we are able to perform both statistical analyses and halo-by-halo comparisons. Our study demonstrates that there is a good statistical agreement between the three models used here, when operating on the same merger trees, reflecting a general agreement in the underlying framework for semi-analytic models. We also show, however, that various assumptions that are commonly adopted to treat gas cooling and galaxy mergers can lead to significantly different results, at least in some regimes. In particular, we find that the different models adopted for gas cooling lead to similar results for mass scales comparable to that of our own Galaxy. Significant differences, however, arise at larger mass scales. These are largely (but not entirely) due to different treatments of the 'rapid cooling' regime, and different assumptions about the hot gas distribution. At this mass regime, the predicted cooling rates can differ up to about one order of magnitude, with important implications on the relative weight that these models give to AGN feedback in order to counter-act excessive gas condensation in relatively massive haloes at low redshift. Different assumptions in the modelling of galaxy mergers can also result in significant differences in the timings of mergers, with important consequences for the formation and evolution of massive galaxies.

**Key words:** galaxies: formation – galaxies: evolution – galaxies: cooling flows – galaxies: interactions.

## 1 INTRODUCTION

Understanding how galaxies form and the physics that drive their evolution has been a long-standing problem in modern astrophysics. A number of observational tests have recently succeeded in determining the fundamental cosmological parameters with uncertainties of only a few per cent, thus effectively removing a large part of the parameter space in galaxy formation studies. We are left, however, with the problem of dealing with our 'ignorance' of complex physical processes, that are inter-twined in an entangled network of actions, back-reactions, and self-regulations.

Over the past decades, different methods have been developed to study galaxy formation in a cosmological context. Among these, semi-analytic models have turned into a flexible and widely used tool to provide detailed predictions of galaxy properties at different cosmic epochs. These techniques find their seeds in the pioneering work by White & Rees (1978), were laid out in a more detailed form in the early 1990s (White & Frenk 1991; Cole 1991; Kauffmann, White & Guiderdoni 1993), and have been substantially extended and refined in the last years by a number of different groups (for a review, see Baugh 2006). In these models, the evolution of the baryonic components is modelled adopting simple yet physical and/or observationally motivated *recipes*, coupled in a set of differential equations that describe the variation in mass as a function of time of different galactic components (e.g. stars, gas, metals).

While it is relatively easy to compare results from differ-

⋆ Email: delucia@oats.inaf.it

ent models[1], it is more complicated to understand the origin of any difference or similarity between them. This difficulty stems primarily from the fact that different groups adopt different sets of prescriptions (that are equally reasonable, given our poor understanding of the physics at play) and that, as mentioned above, the final results are given by a combination of these. There are, however, also a number of more subtle differences that are more 'technical' in nature (e.g. the particular mass definition adopted, the cooling functions used, the use of analytic or numerical merger trees, etc.). The precise influence on models' results of at least some of these details is unclear. For example, it has been shown that the extended Press-Schechter (EPS) formalism (Bond et al. 1991; Bower 1991) does not provide an adequate description of the merger trees extracted directly from numerical simulations (Benson et al. 2005; Cole et al. 2008). Although some of these most recent studies have provided 'corrections' to analytic merger trees, many applications are still carried out using the classical EPS formalism, and little work has been done to understand to which measure this affects predictions of galaxy formation models.

In this paper, we compare results from three independently developed semi-analytic models. Our goal is not to predict or reproduce any specific observation. Rather our aim is to understand the level of agreement between different semi-analytic models, with a minimum of assumptions or free parameters. This requires (1) that the models are implemented on *identical* merger trees, such that results can be compared on a case-by-case basis and any differences can be attributed to *specific parametrizations of physical processes*; and (2) that a minimum of physical processes are included in the models in order to avoid possible degeneracies, and to hopefully illuminate the effects of specific parametrizations or parameter choices.

In our study, the first requirement has been satisfied by creating a standard set of halo merger trees extracted from $N$-body simulations, and running each model on these trees. The second requirement is somewhat more demanding as modern semi-analytic models contain treatment of numerous, coupled physical processes. We have chosen to simplify the models as much as possible by removing *all* physics other than gas cooling and galaxy mergers. This allows us to focus on the influence of different assumptions typically made to model these two physical processes, that represent two basic ingredients of any galaxy formation model. Using large samples of identical haloes, we are able to compare results both in a statistical fashion and on a halo-by-halo basis.

Previous studies (e.g. Benson et al. 2001; Yoshida et al. 2002; Helly et al. 2003; Cattaneo et al. 2007) have compared numerical predictions from stripped-down versions of semi-analytic models with those from hydrodynamical simulations, to verify whether these methods provide consistent predictions in the idealized case in which only gas cooling is included. The general consensus is that the cooling model usually employed in semi-analytic models is in good agreement with hydrodynamical simulations that adopt the same physics. More recent studies focused on object-by-object comparisons, however, have highlighted a number of important differences that were 'hidden' in the relatively good agreement obtained by previous studies focusing on statistical comparisons (Saro et al. 2010). A recent study by Viola et al. (2008), in particular, has shown that the cooling model implemented in MORGANA (one of the models used in this study) predicts cooling rates that are significantly larger than those predicted from their implementation of the 'classical' cooling model, proposed by White & Frenk (1991). In addition, Viola et al. have shown that MORGANA provides results that are in good agreement with those of controlled numerical experiments of isolated haloes, with hot gas in hydrostatic equilibrium. While both SPH and semi-analytic techniques have their own weaknesses, making it unclear which of the two (if either) is providing the 'correct' answer, these results appear confusing. It is therefore interesting to study how the different possible assumptions that can be made to model the evolution of cooling gas, propagate on predictions from galaxy formation models.

Modelling of galaxy mergers has not been considered a major concern, but different assumptions about merging time-scales can be made, and these may have important consequences for the inferred stellar assembly history of massive galaxies, including brightest cluster galaxies. In addition, recent work has shown that the classical dynamical friction formula usually adopted in semi-analytic models tends to under-estimate merging times computed from controlled numerical experiments and high-resolution cosmological simulations (Boylan-Kolchin, Ma & Quataert 2008, Jiang et al. 2008). Results from these studies, however, have not yet converged on the appropriate correction(s) that should be applied to the classical formula.

In this paper, we will not address the issue of what is *the best way* to model galaxy mergers or gas cooling. Instead, we will concentrate on the differences due to alternative implementations of these physical processes, with the aim of understanding their effects in a full semi-analytic model. We will also explore what these effects might imply for the importance of other physical processes.

The numerical simulations and merger trees used in our study are described in Section 2. In Section 3, we describe in detail how gas cooling and galaxy mergers are treated in each of the three models used in this work. Section 4 and Section 5 present our results for two halo samples. In Section 6, we discuss the influence of numerical resolution and of different schemes for the construction of merger trees. Section 7 compares the different implementations of merger times adopted in the three models considered. Finally, we summarize and discuss our results, and give our conclusions in Section 8.

## 2 THE SIMULATIONS AND THE MERGER TREES

This work takes advantage of two large high-resolution cosmological simulations: the *Millennium Simulation* (MS, Springel et al. 2005), and the *Millennium-II* (MS-II, Boylan-Kolchin et al. 2009). The MS follows $N = 2160^3$ particles of mass $8.6 \times 10^8\, h^{-1}\mathrm{M}_\odot$, within a comoving box

[1] A number of galaxy catalogues have been made publicly available by various groups; results from different versions of two of the models used in this study are available through a relational database accessible at:
http://www.mpa-garching.mpg.de/millennium/

| **Name** | $L_{\rm box}$ | $\epsilon$ $[h^{-1}\,{\rm kpc}]$ | $m_p$ $[h^{-1}{\rm M}_\odot]$ |
|---|---|---|---|
| MS | 500 | 5.0 | $8.61 \times 10^8$ |
| MS-II | 100 | 1.0 | $6.89 \times 10^6$ |
| mini-MS-II | 100 | 5.0 | $8.61 \times 10^8$ |

**Table 1.** Some basic properties of the three simulations used in this study: the side length of the simulation box $L_{\rm box}$, the Plummer-equivalent force softening $\epsilon$, and the particle mass $m_p$.

of size $500\,h^{-1}$Mpc on a side. The MS-II follows the evolution of the same number of particles in a volume that is 125 times smaller than for the MS ($100\,h^{-1}$Mpc on a side). The particle mass is correspondingly 125 times smaller than for the MS ($6.9 \times 10^6\,h^{-1}{\rm M}_\odot$), allowing haloes similar to those hosting our Milky Way to be resolved with hundreds of thousands of particles. For both simulations, the cosmological model is a $\Lambda$CDM model with $\Omega_{\rm m} = 0.25$, $\Omega_{\rm b} = 0.045$, $h = 0.73$, $\Omega_\Lambda = 0.75$, $n = 1$, and $\sigma_8 = 0.9$. The Hubble constant is parameterised as $H_0 = 100\,h\,{\rm km\,s^{-1}Mpc^{-1}}$. In order to test how numerical resolution affects our results, we will also use the *mini-Millennium-II* simulation (mini-MSII; Boylan-Kolchin et al. 2009), which was run using the same initial conditions and volume as for the MS-II, but at the mass and force resolution as for the original MS (the number of particles is therefore $432^3$). The basic properties of the three simulations used in this study are summarised in Table 1.

For each simulation snapshot (64 for the MS, 68 for the MS-II), group catalogues were constructed using a standard friends–of–friends (FOF) algorithm, with a linking length of 0.2 in units of the mean particle separation. Each group was then decomposed into a set of disjoint substructures using the algorithm SUBFIND (Springel et al. 2001), which iteratively determines the self-bound subunits within a FOF group. The most massive of these substructures is often referred to as the *main halo*, while this and all other substructures are all referred to as *subhaloes* or *substructures*. Only subhaloes that retain at least 20 bound particles after a gravitational unbinding procedure are considered 'genuine' subhaloes, and are used to construct merger history trees as explained in detail in Springel et al. (2005) (see also De Lucia & Blaizot 2007 and Boylan-Kolchin et al. 2009). The subhalo detection limit is therefore set to $2.36 \times 10^{10}$, and to $1.89 \times 10^8$ M$_\odot$ for the MS and the MS-II, respectively. Note that some FOF haloes do not contain 20 self-bound particles; such FOF haloes are not included in the merger trees.

The comparison discussed below will focus on two samples of haloes. The first sample consists of 100 haloes, selected from the MS-II on the basis of their mass at $z = 0$, with $\log {\rm M}_{200}$ between 11.5 and 12.5. Here ${\rm M}_{200}$ is in units of $h^{-1}{\rm M}_\odot$, and is defined as the mass within a sphere of density 200 times the critical density of the Universe at the corresponding redshift[2]. We will refer to this sample as the 'Milky-Way like' sample. A second sample of other 100 haloes was selected from the MS by taking haloes that have a number density of $10^{-5}$ at $z \sim 2$, and that end up in massive groups/clusters at $z = 0$. The adopted number density is comparable to that of submillimiter galaxies at $z \sim 2$ (Chapman et al. 2004, and references therein). We will refer to this sample as the 'SCUBA-like' sample.

As mentioned above, trees for the MS and MS-II were originally constructed at the subhalo level. Many semi-analytic models, however, are based on FOF merger trees. We have therefore constructed FOF-based merger trees for our halo samples. There are many possible ways to construct FOF merger trees from subhalo trees. We have chosen one of the most straightforward methods: since there exists a one-to-one correspondence between FOF haloes in the subhalo trees and main subhaloes, we are free to assign the merger history of a FOF halo to the merger history of its dominant subhalo. We use this mapping from dominant subhaloes to FOF haloes to directly link the merger history of dominant subhaloes to the merger history of their host FOF haloes. So, for example, if dominant subhalo $\alpha$ of FOF group $A$ has the descendant $\beta$ in FOF group B, then FOF halo $B$ is defined to be the descendant of FOF halo $A$ in our FOF trees.

More sophisticated algorithms for constructing FOF trees from the MS or MS-II subhalo trees exist (e.g. Fakhouri & Ma 2008; Genel et al. 2008). In particular, these algorithms filter out "unphysical" FOF mergers – for example, those due to chance associations of two FOF haloes for only one snapshot. Each of these algorithms has different strengths and weaknesses. The primary virtue of the algorithm we have chosen is its simplicity, and the advantage that each FOF tree can be easily connected to the corresponding subhalo tree (we will use subhalo-based merger trees in Section 6).

## 3 THE MODELS

In this study, we use three different and independently developed semi-analytic codes. In the following, we will refer to them as the *Munich* model, the *Durham* model, and *MORGANA*. As explained above, we have used stripped-down versions of the models that only include gas cooling and galaxy mergers, so as to focus on a few specific aspects of the modelling. In addition, all models have been adapted to run on the merger trees described in Section 2. In the following, we describe in more details how gas cooling and galaxy mergers are treated in each of the models used in our study, and the changes that were made in order to adapt each code to the same merger trees.

### 3.1 The Munich model

The version of the Munich model used in this study is the one described in De Lucia & Blaizot (2007), and we refer to the original paper and references therein for more details.

The rate of gas cooling is computed following the model

[2] The corresponding radius, $R_{200}$, has been shown to approximately demarcate the inner regions of haloes which are in dynamical equilibrium, from the outer regions which are still infalling (Cole & Lacey 1996). In the following, we will refer to this radius as the 'virial radius', $R_{\rm vir}$. The virial mass $M_{\rm vir}$ is the mass contained within the sphere defined by this radius, and the virial velocity $V_{\rm vir}$ is the circular velocity at $R_{\rm vir}$.

originally proposed White & Frenk (1991), and an implementation similar to that adopted in Springel et al. (2001). The Munich model assumes that the hot gas within dark matter haloes follows an isothermal profile:

$$\rho_{\rm g}(r) = \frac{M_{\rm hot}}{4\pi R_{200} r^2}.$$

For each new snapshot, the total amount of hot gas available for cooling in each halo is estimated as follows:

$$M_{\rm hot} = f_{\rm b} M_{\rm vir} - \sum_i M_{\rm cold}^{(i)} \quad (1)$$

where the sum extends over all the galaxies in the FOF halo and $f_{\rm b}$ is the baryon fraction of the Universe, for which we assume the value 0.017[3]. Eq. 1 can provide, in a few cases, a negative number (this occurs typically after important halo mergers). In this case, the amount of hot gas is set to zero, and no cooling is allowed in the remnant halo.

The equations driving galaxy evolution are then solved using 20 time-steps between each pair of simulation snapshots. A local cooling time is defined as the ratio between the specific thermal energy content of the gas and the cooling rate per unit volume:

$$t_{\rm cool}(r) = \frac{3}{2} \frac{kT\rho_{\rm g}(r)}{\bar{\mu} m_{\rm p} n_{\rm e}^2(r) \Lambda(T,Z)} \quad (2)$$

In the above equation, $\bar{\mu} m_{\rm p}$ is the mean particle mass, $n_{\rm e}(r)$ is the electron density, $k$ is the Boltzmann constant, and $\Lambda(T,Z)$ represents the cooling rate. The latter is strongly dependent on the virial temperature of the halo, and on the metallicity of the gas. In the Munich model, these dependencies are accounted for by using the collisional ionization cooling curves by Sutherland & Dopita (1993). Since chemical enrichment is switched off in this study, we only use the calculation corresponding to 'primordial' composition. The virial temperature of the halo is determined using the hydrostatic equilibrium equation, and relates the gas temperature to the circular velocity of the halo:

$$T_{\rm vir} = \frac{1}{2} \frac{\mu m_{\rm H}}{k} V_{\rm vir}^2 \quad \text{or} \quad T_{\rm vir} = 35.9 (V_{\rm vir}/{\rm km\,s^{-1}})^2 \ {\rm K}$$

where $m_{\rm H}$ is the mass of the hydrogen atom, and $\mu$ is the mean molecular mass.

A 'cooling radius' is then computed as the radius at which the local cooling time is equal to the halo dynamical time. We note that in the original work by White & Frenk, the cooling radius was defined equating the local cooling time to the age of the Universe, which is about one order of magnitude larger than the halo dynamical time. As discussed in De Lucia, Kauffmann & White (2004), the particular choice currently adopted in the Munich model was motivated by the significant enhancement of cooling rates when adopting metal dependent cooling functions.

If the cooling radius lies within the virial radius of the halo under consideration, the gas is assumed to cool quasi-statically, and the cooling rate is modelled by a simple inflow equation:

$$\frac{{\rm d}M_{\rm cool}}{{\rm d}t} = 4\pi \rho_{\rm g}(r_{\rm cool}) r_{\rm cool}^2 \frac{{\rm d}r_{\rm cool}}{{\rm d}t}$$

[3] In this work, all models assume the same value for the universal baryon fraction.

At early times, and for low-mass haloes, the formal cooling radius can be much larger than the virial radius. In this case, the infalling gas is never expected to come to hydrostatic equilibrium, and the supply of cold gas for star formation is limited by the infall rate. In this 'rapid cooling regime', we assume that all new diffuse gas that is accreted onto the halo is immediately made available for star formation in the central galaxy of the halo under consideration.

In its standard implementation, the Munich model follows explicitly dark matter haloes when they are accreted onto larger systems. This allows the dynamics of satellite galaxies residing in infalling structures to be properly followed, until their parent dark matter substructures are completely destroyed by tidal truncation and stripping (e.g. De Lucia et al. 2004). When this happens, galaxies are assigned a residual surviving time that is estimated from the relative orbit of the two merging objects, at the time of subhalo disruption, using the following implementation of the Chandrasekhar dynamical friction formula:

$$\tau_{\rm merge} = f_{\rm fudge} \frac{1.17}{\ln \Lambda_{\rm df}} \frac{D^2}{R_{\rm vir}^2} \frac{M_{\rm main}}{M_{\rm sat}} \tau_{\rm dyn} \quad (3)$$

In the above equation, $D$ is the distance between the merging halo and the centre of the structure on which it is accreted, $R_{\rm vir}$ is the virial radius of the accreting halo, $M_{\rm sat}$ is the (dark matter) mass associated with the merging satellite, and $M_{\rm main}$ is the (dark matter) mass of the accreting halo. The dynamical time of the halo, $\tau_{\rm dyn}$, is given by

$$\tau_{\rm dyn} = \frac{R_{\rm vir}}{V_{\rm vir}} = \left( \frac{R_{\rm vir}^3}{G\, M_{\rm vir}} \right)^{1/2}. \quad (4)$$

Note that with the definition of virial mass adopted here, $\tau_{\rm dyn} = 0.1/H(z)$ and is independent of the halo mass. The Coulomb logarithm $\Lambda_{\rm df}$ is taken to be $1 + M_{\rm main}/M_{\rm sat}$.

For the purposes of this analysis, we have used Eq. 3 also for FOF-based merger trees, without adding any additional orbital dependence, and using $R_{\rm vir}$ in place of $D$. As in De Lucia & Blaizot (2007), we have assumed $f_{\rm fudge} = 2$. This was originally introduced to reduce the slight excess of bright galaxies otherwise produced, and was motivated by some preliminary work by Springel et al. (2001), who noted that merging times inferred from Eq. 3 are typically shorter than those directly measured using higher resolution numerical simulations. As mentioned in Section 1, more recent work has confirmed that the classical dynamical friction formula tends to under-estimate merging times (Boylan-Kolchin et al. 2008; Jiang et al. 2008). While these studies have not yet converged on the proper adjustment(s) to the classical dynamical friction formulation, they suggest that the appropriate correction(s) cannot be absorbed in a fudge factor in front of Eq. 3. For example, while the fudge factor adopted in De Lucia & Blaizot (2007) is in good agreement with findings from Boylan-Kolchin et al. (2008) for $M_{\rm sat}/M_{\rm host} \approx 0.1$, it is significantly lower than what found for smaller mass ratios.

### 3.2 The Durham model

The version of the Durham model used in this study is described in Bower et al. (2006). For full details on the cooling and merging times modelling, the reader is referred to Benson et al. (2003) and Cole et al. (2000). A few small

modifications were necessary in order to make the model run on the merger trees described in Section 2. These are briefly discussed below.

The hot gaseous component in dark matter haloes is assumed to have a density profile described by the $\beta$-model:

$$\rho_{\rm g}(r) = \frac{\rho_0}{[1+(r/r_{\rm core})^2)]^{3\beta/2}}$$

where $\rho_0$ is the density at the centre of the halo, $r_{\rm core}$ is the radius of the core, and $\beta$ is a parameter that sets the slope of the profile at radii larger than $r_{\rm core}$. The model assumes a gas density profile with $r_{\rm core} = 0.07 \cdot R_{\rm vir}$ and $\beta = 2/3$ for all haloes, in absence of energy injection (Benson et al. 2003). Since feedback is switched off in this study, these are the model parameters adopted for our comparison. The temperature profile of the gas is assumed to be isothermal at the virial temperature.

A set of 'halo formation events' are defined throughout each merger tree, and cooling calculations are begun and reset at these formation events. In particular, each halo with no progenitor is flagged as a 'formation event'. For all other haloes in the tree, a 'formation event' flag is assigned to all those for which their mass is equal to, or larger than, twice the mass of the halo at the previous formation event in that branch. For these haloes then, formation events correspond to halo mass doublings.

At each new snapshot, the mass of gas that falls onto the halo is given by:

$$M_{\rm infall} = \max\left[(M_{\rm vir} - \sum_i M^i_{\rm vir}) \cdot f_{\rm b}, 0.0\right]$$

where the sum extends over all the progenitors of the halo under consideration. Although $M_{\rm infall}$ is accumulated for each snapshot, it is only added to the hot gas of the halo at a formation event.

As for the Munich model, the following calculations are then done using 20 time-steps between each pair of simulation snapshots. A local cooling time is defined using Eq. 2, and the metal free cooling function computed from CLOUDY v8.0 (Ferland et al. 1998). A cooling radius is then computed by equating the local cooling time to the time since the last formation event (the cooling radius is not allowed to exceed the virial radius). An infall radius is also computed, as the minimum between the cooling radius and the free-fall radius (i.e. the radius within which gas has had time to fall ballistically to the halo centre, assuming that it began at rest at the previous formation event). The mass of gas that infalls onto the central galaxy during each time-step is finally computed as the difference between the hot gas enclosed within the current infall radius and the mass that was inside the infall radius at the previous time-step.

Galaxy mergers are treated in a way similar to that done in the Munich model, with a few differences. When a new halo forms, each satellite is assumed to enter the halo on a random orbit (the most massive pre-existing galaxy becomes the central galaxy of the remnant halo). The dynamical friction formulation adopted in the Durham model is given in Cole et al. (2000) and reads as:

$$\tau_{\rm merge} = f_{\rm fudge}\,\Theta_{\rm orbit}\,\frac{0.3722}{\ln\Lambda_{\rm df}}\,\frac{M_{\rm main}}{M_{\rm sat}}\,\tau_{\rm dyn} \qquad (5)$$

where $M_{\rm halo}$ is the mass of the halo in which the satellite orbits, and $M_{\rm sat}$ is the mass of the satellite galaxy including the mass of the dark matter halo in which it formed. The Coulomb logarithm $\Lambda_{\rm df}$ is taken to be $M_{\rm halo}/M_{\rm sat}$. The orbital dependence is contained in $\Theta_{\rm orbit}$, modelled as a log-normal distribution with mean $< \log\Theta_{\rm orbit} >= -0.14$ and dispersion $< (\log\Theta_{\rm orbit} - < \log\Theta_{\rm orbit} >)^2 >^{1/2} = 0.26$. Bower et al. (2006), and the stripped-down version used in this study, assume the value 1.5 for the dimensionless parameter $f_{\rm fudge}$. Merger times are reset at each formation event, re-extracting orbital parameters for each satellite.

### 3.3 MORGANA

All details about the modelling of gas cooling and galaxy mergers adopted in MORGANA can be found in Monaco, Fontanot & Taffoni (2007), and we refer to this paper for full details. We note that in its original formulation, MORGANA uses merger trees obtained using PINOCCHIO (Monaco et al. 2002). This algorithm, based on Lagrangian perturbation theory, has been shown to provide mass assembly histories of dark matter haloes that are in excellent agreement with results from numerical simulations (Li et al. 2007). For the purposes of this study, we have adapted MORGANA to run on the numerical merger trees described in Section 2. This required some small modifications that are described below. We note that PINOCCHIO does not provide information on dark matter substructures, so MORGANA is essentially based on FOF merger trees.

The hot halo phase is assumed to be spherical, in hydrostatic equilibrium in a NFW halo, described by a polytropic equation of state with index $\gamma_p = 1.15$, and is assumed to fill the volume between the cooling radius and the virial radius of the halo, where it is pressure balanced. The equilibrium configuration of the hot halo gas is computed at each time-step, assuming that the gas re-adjusts quasi-statically to the new equilibrium configuration, in absence of major mergers. Under these assumptions, one obtains:

$$\rho_{\rm g}(r) = \rho_{g0}\left(1 - a\left(1 - \frac{\ln(1+c_{\rm nfw}x)}{c_{\rm nfw}}\right)\right)^{1/(\gamma_p-1)}$$

$$T_{\rm g}(r) = T_{g0}\left(1 - a\left(1 - \frac{\ln(1+c_{\rm nfw}x)}{c_{\rm nfw}}\right)\right)$$

where

$$a = \frac{3(\gamma_p-1)}{\eta_0\gamma_p}\left(\frac{c_{\rm nfw}(1+c_{\rm nfw})}{(1+c_{\rm nfw})\ln(1+c_{\rm nfw}) - c_{\rm nfw}}\right)$$

In the above equations, $c_{\rm nfw} = r_{\rm halo}/r_s$, and $x = r/r_s$, where $r_s$ is the scale radius of the NFW halo. The constants $\rho_{g0}$ and $T_{g0}$ are defined as the extrapolations to $r = 0$ of the density and temperature profile, while $\eta_0$ is the extrapolation to $r = 0$ of the function $\eta(r) = T_{\rm g}(r)/T_{\rm vir}$. The halo virial temperature $T_{\rm vir}$ is defined as $1/3\mu m_{\rm H} V^2_{\rm vir}/k$.

At each new snapshot, the mass of gas that falls onto the halo is computed as:

$$M_{\rm infall} = f_{\rm b} \cdot \max\left[M_{\rm vir} - (\sum_i M^i + M^{\rm max}_{\rm vir}), 0.0\right]$$

where the sum extends over all progenitors of the halo that are not its main progenitor, and $M^{\rm max}_{\rm vir}$ is the maximum virial mass of the main progenitor, considering all previous snapshots. The infall rate of new gas is assumed to be constant

over the time interval between each pair of simulation snapshots. The equations below are then solved using a Runge-Kutta integrator with adaptive time-steps.

The cooling rate of a shell of gas of width $\Delta r$, at a radius $r$, is computed as:

$$\Delta\left(\frac{dM_{\rm cool}(r)}{dt}\right) = \frac{4\pi r^2 \rho_{\rm g}(r)\Delta r}{t_{\rm cool}(r)}$$

where $t_{\rm cool}$ is the local cooling time, computed as in Eq. 2. As in the Munich model, cooling rates are computed using the collisional ionization cooling curves by Sutherland & Dopita (1993), with primordial composition. The mass deposition rate is then computed by summing up the contributions from all mass shells. The summation is carried our by taking into account the radial dependence of the gas density, and provides the following total mass deposition rate:

$$\frac{dM_{\rm cool}}{dt} = \frac{4\pi r_s^3 \rho_{g0}}{t_{\rm cool,0}} \int_{r_{\rm cool}/r_s}^{c_{\rm nfw}} \left[1 - a\left(1 - \frac{\ln(1+t)}{t}\right)\right]^{2/(\gamma_p - 1)} t^2 dt$$

where $t_{\rm cool,}0$ is computed using the central density $\rho_{g0}$ and the temperature of the gas at $r_{\rm cool}$.

Finally, by equating the mass cooled in a time interval $dt$ with the mass contained in a shell $dr$, one obtains the evolution of the cooling radius, that is treated as a dynamical variable in this model:

$$\frac{dr_{\rm cool}}{dt} = \frac{dM_{\rm cool}/dt}{4\pi\rho_{\rm g}(r_{\rm cool})r_{\rm cool}^2} - c_{\rm s}$$

where $c_{\rm s}$ is the sound speed computed at $r_{\rm cool}$, and is added to the right hand side of the above equation to allow the 'cooling hole' to close at the sound speed.

The cooling calculation is started when a halo appears for the first time, with $r_{\rm cool} = 0.001 \cdot r_s$, and is reset after any halo major merger ($M_{\rm sat}/M_{\rm main} > 0.2$). Finally, cooled gas is incorporated onto the central galaxy at the following rate:

$$\frac{dM_{\rm cold}}{dt} = \frac{M_{\rm cooled}}{n_{\rm dyn}\tau_{\rm dyn}(r_{\rm cool})}$$

where $n_{\rm dyn}$ is treated as a free parameter (we assume a value of 0.3 for this parameter, as in the standard MORGANA model) and represents the number of dynamical times, computed at the cooling radius, required for the cooled gas to be incorporated onto the central galaxy. In the comparison discussed below, the above delay in the incorporation of the cooled gas is neglected.

When a halo is accreted on a larger structure, orbital parameters are extracted randomly from suitable distributions that are based on results from numerical simulations. In particular, the eccentricity of the orbit ($\epsilon = J/J_c$, where $J$ is the initial angular momentum of the orbit and $J_c$ is the angular momentum of a circular orbit with the same energy) is extracted from a Gaussian with mean 0.7 and variance 0.2, while the energy of the orbit ($x_c = r_c/r_h$, where $r_h$ is the halo radius and $r_c$ is the radius of a circular orbit with the same energy) is assumed to be 0.5 for all orbits. To model galaxy mergers, Monaco et al. (2007) use a slight update of the formulae provided by Taffoni et al. (2003), that take into account dynamical friction, mass loss by tidal stripping, tidal disruption of subhaloes, and tidal shocks. Galaxy merger times are computed interpolating between the case for a 'live satellite' (the object is subject to significant mass losses) and that of a 'rigid' satellite (no mass loss):

$$\tau_{\rm merge,live} = \frac{\tau_{\rm dyn}}{f_{\rm sat}} \left(\xi_1 f_{\rm sat}^{0.12} + \xi_2 f_{\rm sat}^2\right) \times \left(0.25\, f_{\rm nfw}^{-6} + 0.07 f_{\rm nfw} + 1.123\right)\left(0.4 + \xi_3(\epsilon - 0.2)\right)$$

$$\tau_{\rm merge,rigid} = 0.46\, \frac{\tau_{\rm dyn}}{f_{\rm sat}} \cdot (1.7265 + 0.0416\, c_{\rm nfw})\, \frac{x_c^{1.5}}{\ln\Lambda_{\rm df}} \qquad (6)$$

In the above equations, $f_{\rm sat} = M_{\rm sat}/M_{\rm vir}$ and $f_{\rm nfw} = c_{\rm sat}/c_{\rm nfw}$. $M_{\rm sat}$ and $c_{\rm sat}$ are the corresponding virial quantities for the satellite halo, and $\xi_i$ are polynomial functions of $x_c$, whose expressions can be found in appendix A of Monaco et al. (2007). The Coulomb logarithm is given by $\Lambda_{\rm df} = 1 + 1/f_{\rm sat}$. Merger times are reset after each halo major merger, re-extracting orbital parameters for each satellite galaxy.

### 3.4 Model differences and similarities

The previous sections illustrate that the implementations of gas cooling and galaxy mergers in the three models used in this study differ in a number of details. Both the Durham and the Munich models adopt variations of the original cooling model proposed by White & Frenk (1991), but they use different gas profiles, and different definitions of the 'cooling time' (used to calculate the cooling radius). In addition, the cooling calculation is reset in the Durham model at each 'formation event', and the Munich model assumes very efficient cooling in the rapid cooling regime. Finally, cosmological infall of gas onto the halo occurs at a constant rate between each pair of snapshots in the Munich model, while occurs at formation events for the Durham model. A cored density profile, like the one adopted in the Durham model, is expected to give lower cooling rates than an isothermal profile. It is not clear, however, how this naive expectation is affected by the other different assumptions discussed above.

The adopted modelling for merger times is also very similar in the Durham and Munich models, as well as for the 'rigid' case in the MORGANA model. Indeed, by comparing Eqs. 3, 5, and 6 with $D = R_{\rm vir}$ in the Munich model, $\Theta_{\rm orbit} = 1$ in the Durham model, and $c_{\rm NFW} = 10$ in (the rigid version of) MORGANA, the implementations differ only in the numerical pre-factor (Munich: $1.17\, f_{\rm fudge}$; Durham: $0.3722\, f_{\rm fudge}$; MORGANA: 0.348) and in the implementation of the Coulomb logarithm. (The full 'live' version of dynamical friction in MORGANA is somewhat more complicated.)

MORGANA differs significantly from the Durham and the Munich models, both in its gas cooling and merger times implementations. As explained above, in the Durham and Munich model the cooling radius is computed by equating the local cooling time (Eq. 2) to some given time (the halo dynamical time in the Munich model and the time since the last formation event in the Durham model). MORGANA computes the cooling rate at each mass shell, integrates over the contribution of all shells, and follows the evolution of the cooling radius by assuming that the transition from the hot to the cold phase is fast enough to create a sharp edge in the density profile of the hot gas. The cooling radius 'closes' at the sound speed.

As mentioned in Section 1, Viola et al. (2008) have

shown that results from this model are in good agreement with controlled hydrodynamical simulations of isolated haloes, with hot gas in hydrostatic equilibrium in a NFW halo. Viola et al. have also shown that their implementation of the classical model underpredicts the amount of gas cooling with respect to the model adopted in MORGANA, particularly at early times. Their implementation of the 'classical' model differs in detail from those adopted in the Munich and Durham models, however. In addition, it is unclear that results obtained from their controlled simulations should remain valid when using cosmologically motivated halo merger histories, as done in this study. The formulation adopted to model dynamical friction in MORGANA is based on controlled simulations and analytic models, and takes into account dynamical friction, mass loss by tidal stripping, tidal disruption of subhaloes, and tidal shocks. Since the other two models treat satellites as rigid systems, they are expected to provide somewhat shorter merger times. We will come back to a more detailed comparison between the adopted formulations in Section 7.

MORGANA and the Munich model compute cooling rates using results by Sutherland & Dopita (1993), while the Durham model adopts updated rates computed using CLOUDY. We have verified that the metal free cooling function computed using CLOUDY does not differ significantly from the primordial cooling function from Sutherland & Dopita (1993). It should be noted, however, that this is not the case for non-zero metallicities, where the Sutherland & Dopita calculation tends to over-estimate the cooling rates computed using CLOUDY.

Finally, we note that in all three models used in this study, gas cooling occurs only on central galaxies. When galaxies are accreted onto a more massive system, their hot reservoir is assumed to be instantaneously stripped and associated with the parent halo of the remnant central galaxy.

## 4 MILKY-WAY HALOES

In this section we will analyse results of the three models described above for a sample of Milky-Way like haloes. As discussed in Section 2, these haloes have been selected only on the basis of their present virial mass, with no additional constraint on their merger history or isolation. An in-depth analysis of the full sample of Milky Way-mass haloes in the MS-II (comprised of over 7600 haloes) is presented in Boylan-Kolchin et al. (2010).

Fig. 1 shows the dark matter mass scaled by the universal baryon fraction (top panel), the evolution of the cold gas (second panels from top) and hot gas (third panels from top) components associated with the central galaxy, and the cooling rate (bottom panels) for two MW-like haloes. The cold and hot components have been normalized by the dark matter mass of the parent halo, which is the same in all three models by construction. Red, green and blue lines show results from the Durham, Munich and MORGANA models, respectively. The haloes chosen for this figure provide two representative examples for a MW halo with a rather quiet mass accretion history (left panels) and one with a larger number of massive mergers (right panels). To avoid complications arising from a different treatment of merging times, the evolution of the cold gas content is shown for both $t_{mrg} = \infty$ (solid lines) and $t_{mrg} = 0$ (dashed lines). The amount of hot gas associated with the central galaxy, as well as the cooling rate, are not affected by the particular merging model adopted, because the hot gas associated with galaxies falling onto a larger system (i.e. becoming satellites) is instantaneously stripped and associated with the hot gas component of the main halo, in all three models.

Fig. 1 shows a quite good degree of agreement between the three models used in this study. At high redshift, when the halo is in a rapid accretion regime, a large fraction of its baryonic mass is converted into cold gas in the Munich model and in MORGANA, while cooling appears to be less efficient in this regime in the Durham model. By redshift $\sim 7-9$, all models converge to about the same cold gas and hot gas fractions. At lower redshift, the evolution of both components is very similar, with small differences between different models at present (see below). As expected, the evolution of both baryonic components is more noisy for the halo whose mass accretion history is characterized by a larger number of important mergers. In particular, the Durham model shows a quite noisy behaviour in the hot gas evolution, which is due to the fact that gas infalling onto the halo is added to the hot gas component only at 'formation events' (see Section 3). For the halo shown in the right panels, the differences between the amounts of cold and hot gas predicted by the three models are somewhat larger than for the halo with a smoother accretion history shown in the left panels, and differences appear to accumulate at each merger event.

The predicted cooling rates are very noisy for all three models used in this study, and in both examples shown in Fig. 1. In these, the highest cooling rates are obtained in the Durham model and are of the order of $\sim 1.8 \times 10^{10}\,\mathrm{M_{\odot}Gyr^{-1}}$. In a number of the other haloes in the MW sample, cooling rates as high as about twice this value are obtained, and there is some tendency for the Durham model to provide the noisiest behaviour, in particular at very low redshift ($z < 0.5$). Overall, however, the evolution of the cooling rates predicted by the three models is quite similar.

In order to study any systematics in the evolution predicted by the three models used in this study, we have run each code on the total sample of 100 MW-like haloes. Fig. 2 shows the average evolution of the cold (left panel) and hot (middle panel) gas components associated with the central galaxy, and of the cooling rate (right panel). In the left panel, solid and dashed lines correspond to the $t_{mrg} = \infty$ and $t_{mrg} = 0$ run, respectively. Red, green and blue lines show again results from the Durham, Munich and MORGANA models, respectively. The fraction of cold gas associated with the central galaxy rises steeply in all models and at progressively decreasing redshift for the Munich model, MORGANA, and for the Durham model. The later evolution of this component is very similar in all three models when merger times are set to zero, with a slight tendency for the Munich model to predict the largest cold gas fraction and the lowest hot gas fraction at present (see below). When merger times are set to $\infty$, the Munich model predicts the highest cold gas fractions at early times and the lowest cold gas fractions at low redshift. MORGANA has a similar behaviour but the cold gas fraction rises slightly later than in the Munich model at early times, and is slightly larger than predicted by the Munich model at late times. Finally, in the

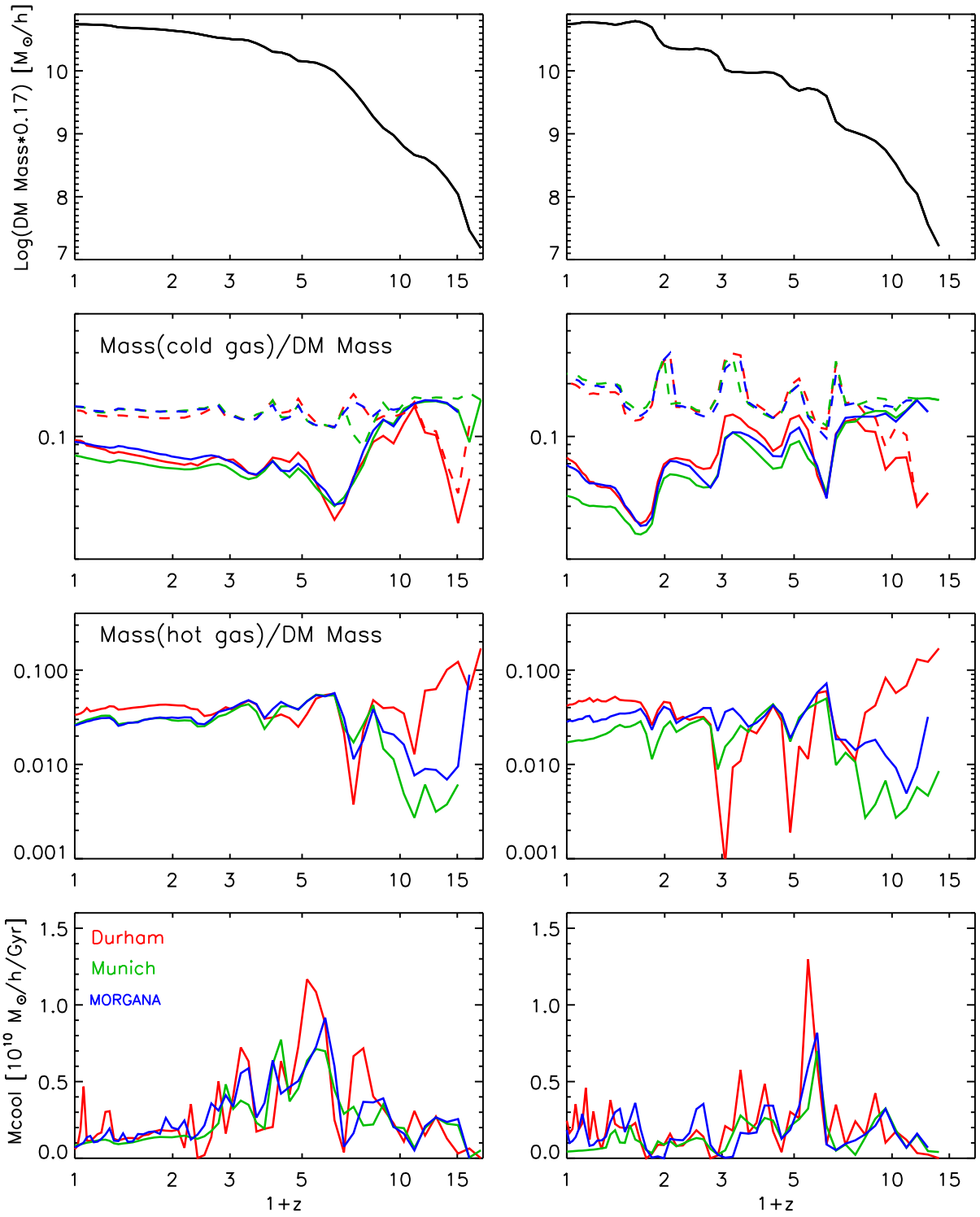


**Figure 1.** From top to bottom: dark matter, cold gas, hot gas, and gas cooling rate for two MW-like haloes. Only quantities associated with the central galaxy and its main progenitors are plotted. Red lines show results from the Durham model, green lines show results from the Munich model and blue lines are for MORGANA. Solid and dashed lines in the second panels from the top show results for the $t_{mrg} = \infty$ and $t_{mrg} = 0$ run, respectively. The haloes shown in this figure provide two representative examples for a halo with a rather quiet mass accretion history (left panels) and a halo with a larger number of massive mergers (right panels).

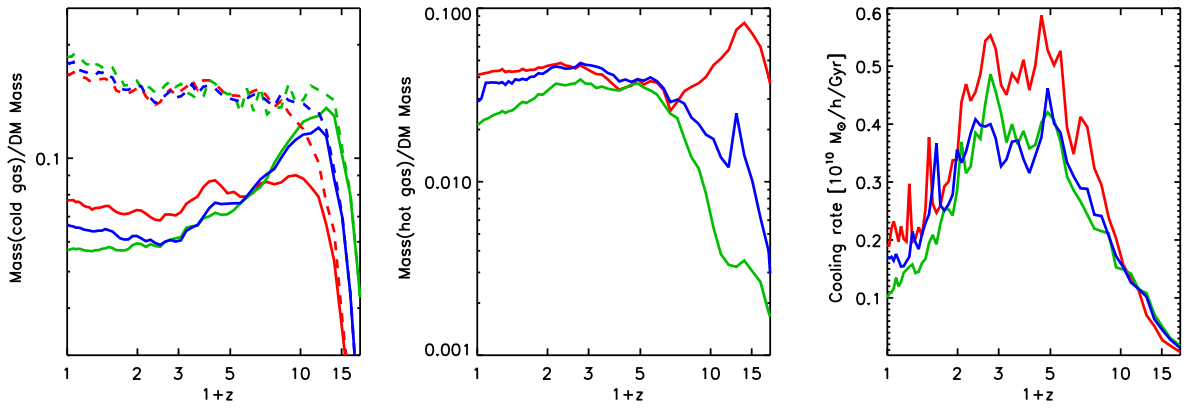


**Figure 2.** From left to right: cold gas, hot gas, and gas cooling between two subsequent snapshots. Each line shows the average computed over 100 MW-like haloes. Solid and dashed lines in the left panels show results for the $t_{mrg} = \infty$ and $t_{mrg} = 0$ run, respectively. Colour-coding is as in Fig. 1.

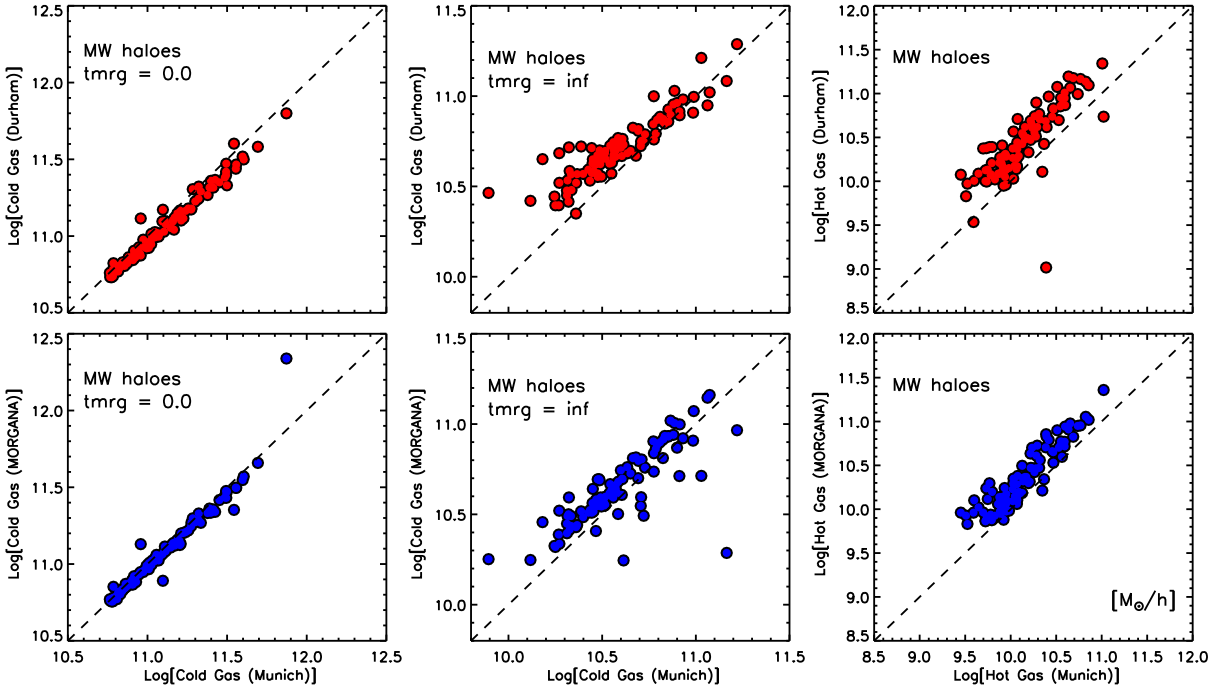


**Figure 3.** Cold gas for the $t_{mrg} = 0$ case (left panels), cold gas for the $t_{mrg} = \infty$ case (middle panels) and hot gas (right panels) associated with the central galaxy for the MW sample. Top panels show results obtained by the Durham code against those from the Munich model. Bottom panels show results by the MORGANA code against those from the Munich model. The dashed line is the one-to-one relation and is plotted to guide the eye.

Durham model, the cold gas fraction starts rising at $z \sim 15$, reaches values of $\sim 0.09$ at $z \sim 10$, and stays almost constant down to $z = 0$. The evolution of the hot gas fraction reflects that of the cold component at high redshift, with the Durham model predicting the largest hot gas fractions, due to a less efficient cooling with respect to the other two models. At $z < 4$, the Durham model is on average still slightly above the predictions from the Munich model and from MORGANA. On average, the Durham model predicts the highest cooling rates in the redshift interval $2-4$. Predictions from the Munich model and from MORGANA are very similar, with a broad peak over the same redshift interval, and with a rapid decline at $z < 2$.

Fig. 3 shows the amount of cold (left panels for $t_{mrg} = 0$ and middle panels for $t_{mrg} = \infty$) and hot gas (right panels) for all MW-like haloes in our sample, at $z = 0$. Top and bottom panels compare the Durham model and MORGANA with the Munich model, respectively. The agreement between the Munich model and MORGANA is very good for the predicted cold gas, particularly when zero merging times

are adopted, with only a very slight tendency for MORGANA to predict a smaller gas content with respect to the Munich model. When suppressing galaxy mergers ($t_{mrg} = \infty$), the agreement is still good, but the scatter is much larger and there is a systematic trend for larger cold gas amounts in MORGANA. The examples discussed above suggest that this might be due to a different treatment of the rapid accretion regime in these two models. The same systematic trend is visible for the hot gas content (right panel), which is always larger in MORGANA than in the Munich model. The trends are similar with the systematics being slightly stronger in the top panels, that compare prediction from the Durham model to those from the Munich model. This figure demonstrates that all three models used in this study provide very similar predictions at present, but that there are some residual systematic trends at late times, and the evolution at high redshift is quite different (see Fig. 1 and Fig. 2).

## 5 SCUBA HALOES

In order to investigate how the level of agreement between different models discussed in the previous section depends on halo mass, we have complemented our MW-like sample with a sample of SCUBA-like haloes. As discussed in Section 2, these have been selected as haloes with a number density of $10^{-5}$ at $z \sim 2$ and with a relatively massive descendant at $z = 0$ ($M_{200} = 7.8 \times 10^{13} - 1.3 \times 10^{15}\, M_{\odot}$). Our decision to use a SCUBA-like sample has been partially motivated by previous claims that MORGANA provides a good agreement with the observed redshift distribution and number counts of 850-$\mu$m sources because the adopted cooling model predicts significantly larger cooling rates with respect to the 'classical' cooling model (Fontanot et al. 2007; Viola et al. 2008). At this mass scale, we therefore expect significant differences between predictions from MORGANA and those from the Munich and Durham models, that both adopt different implementations of the classical model.

Fig. 4 shows the evolution of the cold and hot components (second and third panels from the top) normalized to the parent halo dark matter mass, and of the cooling rates for two examples from our SCUBA sample. As for Fig. 1, these two examples have been chosen as representative for a halo with a rather quiet mass accretion history (left panels), and one with a larger number of important mergers (right panels). The dark matter mass accretion histories of the haloes under consideration are shown in the top panels. Contrary to what expected, predictions from MORGANA appear to be very close to those from the Munich model, while the Durham model deviates most from the other two, predicting systematically lower cold gas fractions at late times. The systematics are stronger when satellite galaxies are allowed to survive as independent entities down to $z = 0$ ($t_{mrg} = \infty$).

The bottom panels of Fig. 4 show that the Durham model predicts much lower cooling rates than the Munich model and MORGANA, below $z \sim 4$. Over this redshift range, both the Munich model and MORGANA provide cooling rates as high as $\sim 80 - 100 \times 10^{10}\, \mathrm{M_{\odot}Gyr^{-1}}$ in the two examples shown; values about twice (or more) as high are obtained in a number of the other haloes from the SCUBA sample. The behaviour predicted by the Munich model for these haloes appears to be somewhat noisier than that predicted by MORGANA, with cooling rates that are not, however, significantly lower. At the highest redshifts probed by the merger trees at disposal, the hot gas fraction predicted by the Munich model is lower than the corresponding value predicted by the Durham model and MORGANA. As noted in the previous section, this results from a very efficient cooling in the rapid accretion regime, as treated by the Munich model. The evolution of the hot gas fraction is then very similar in all three models, down to $z \sim 2$. At redshift lower than this, the Munich model and MORGANA still provide reasonably close results, while the Durham model is systematically higher.

The differences discussed above are clearly visible in Fig. 5, that shows the average evolution of the cold (left panel) and hot (middle panel) gas fractions associated with the central galaxy, and of the cooling rates, computed using all 100 haloes in the SCUBA sample. As in previous figures, solid and dashed lines in the left panel correspond to the $t_{mrg} = \infty$ and $t_{mrg} = 0$ run, respectively. When satellite galaxies are merged immediately after their accretion, the cold gas fractions predicted by the Munich model and MORGANA are very similar at all redshifts, while the Durham model tends to predict larger cold gas fractions at high redshift and lower fractions at $z < 2$. When satellite mergers are suppressed (i.e. satellite galaxies survive as independent entities, keeping the cold gas associated with them before accretion), the Durham model predicts significantly lower cold gas fractions than the Munich model and MORGANA. This is due to the significantly lower cooling rates predicted by the Durham model, as can be seen in the right panel of Fig. 5. This panel shows that, on average, the Munich model predicts the highest cooling rates on this mass scale, while predictions from MORGANA are intermediate between the Munich and Durham models. The middle panel of Fig. 5 shows the evolution of the hot gas fraction, normalized by the corresponding dark matter mass. It shows that, as noted for the MW-like haloes, the cooling efficiency at high redshift is highest in the Munich model. This produces the rapid increase of cold gas visible in the left panel, and is due to a different treatment of the rapid cooling regime in this model. At $z < 2$, the Durham model predicts the largest hot gas fraction and the Munich model the lowest, with MORGANA again providing intermediate results.

The amount of cold and hot gas for all haloes in our SCUBA sample at present are shown in Fig. 6, that compares predictions from Durham model and from MORGANA with results from the Munich model. From this figure, it is clear that there is a systematic trend for both the Durham model (top panel) and MORGANA (bottom panels) to predict lower cold gas fractions and higher hot gas fractions with respect to the Munich model. The disagreement is stronger for the Durham model than for MORGANA, and when galaxy mergers are suppressed. As shown above, this is due to systematic differences in cooling rates, which appear to be more significant for this mass scale than for MW-like haloes (compare right panels in Fig. 5 and Fig. 2).

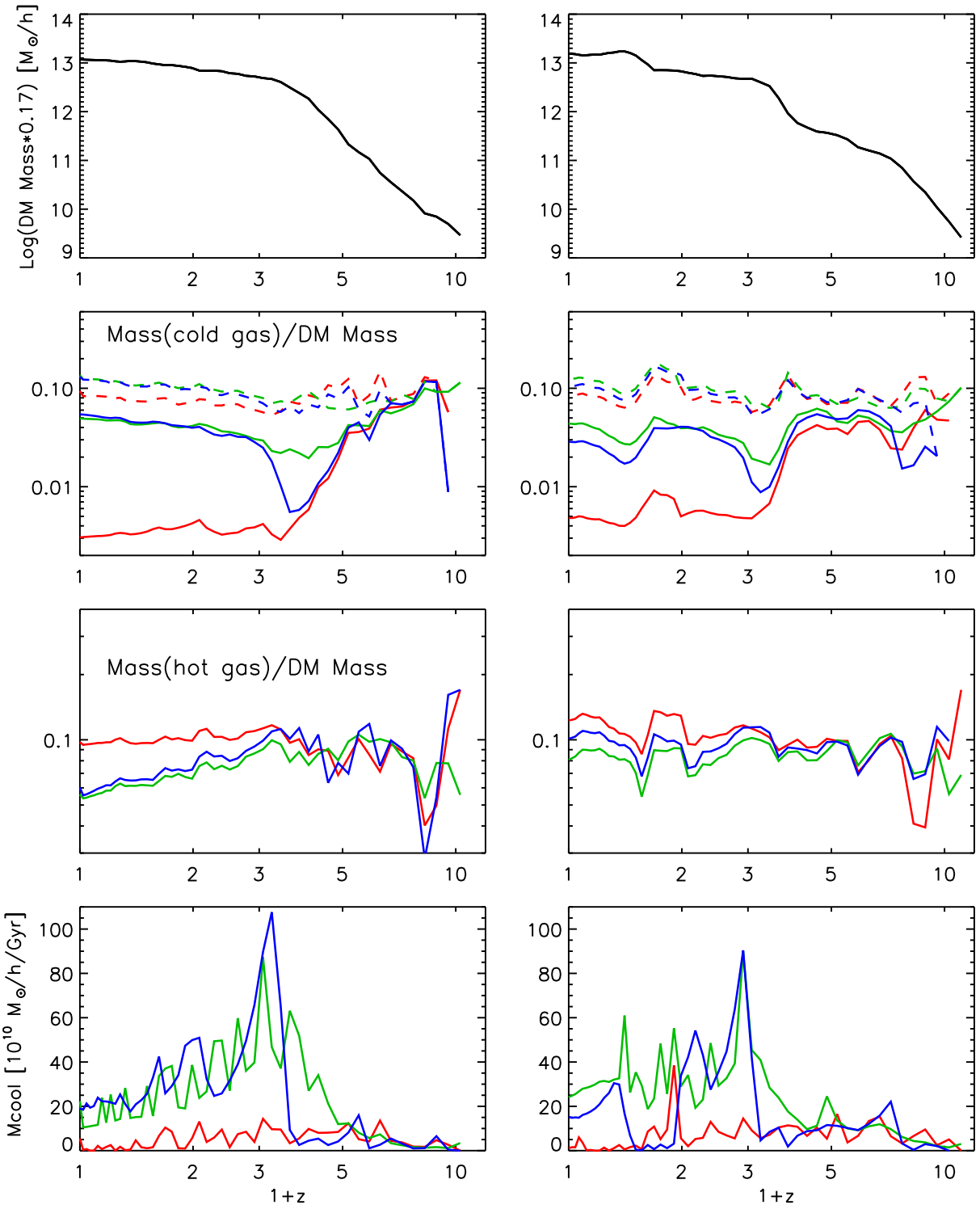


**Figure 4.** Same as in Fig. 1, but for two SCUBA-like haloes.

## 6 NUMERICAL RESOLUTION AND SUBHALO SCHEMES

In order to study how the results discussed in previous sections are affected by numerical resolution, we have taken advantage of the mini-MSII. As explained in Section 2, this simulation has been run with the same initial conditions of the MS-II, but lower force and mass resolution (the same as for the MS). We have identified the *same* haloes used in our MW-sample and run each model on the corresponding merger trees. Haloes were matched across the two simulations by finding, at $z = 0$, all FOF groups in the mini-MS-II within a distance of 1Mpc $h^{-1}$ of the coordinates of the tar-

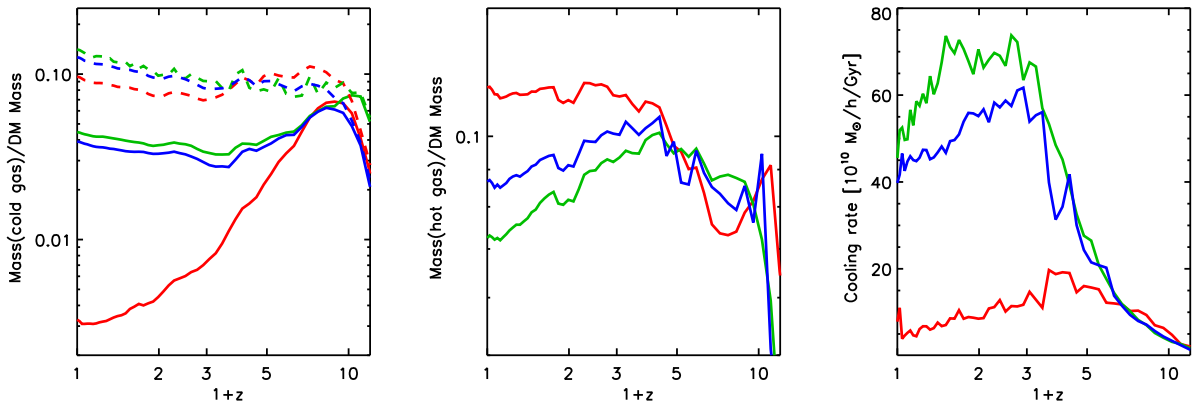


**Figure 5.** Same as in Fig. 2, but for the SCUBA sample.

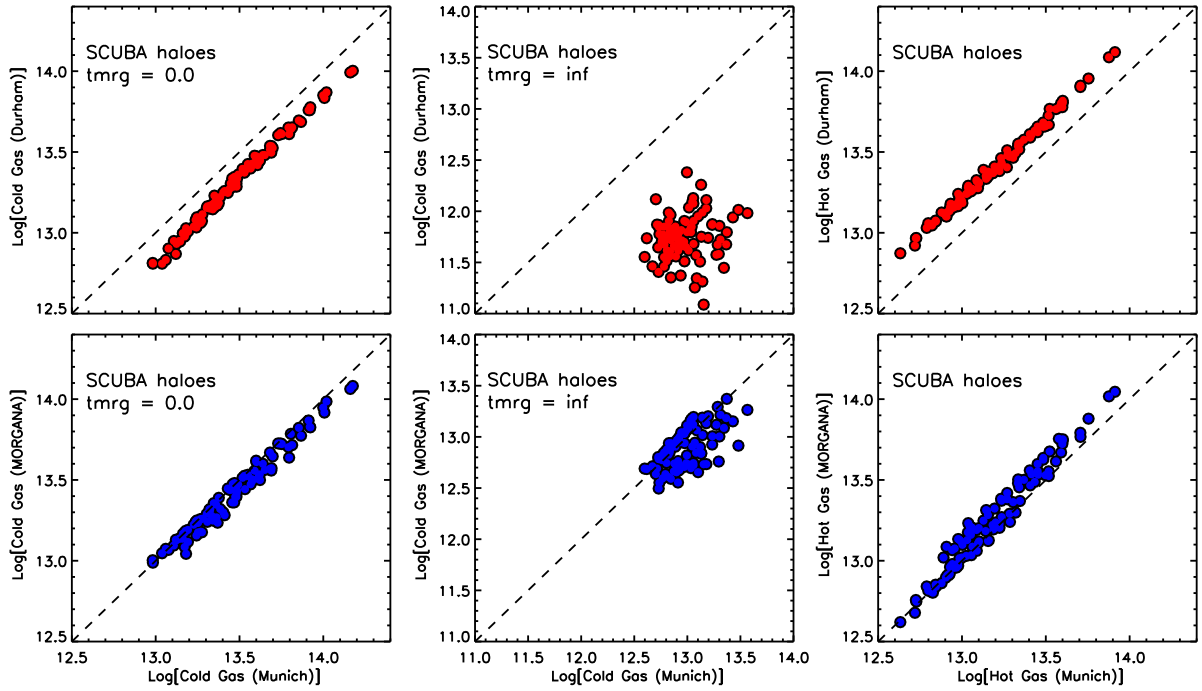


**Figure 6.** Same as in Fig. 3, but for the SCUBA sample. The dashed line is the one-to-one relation and is plotted to guide the eye.

get haloes from the MS-II[4]. For each halo in the original MW sample, the matched halo is found from this subset of haloes, as the one that minimizes the absolute value of $M_{\rm vir}$(mini-MSII)/$M_{\rm vir}$(MS-II)$-1$. We find that the matched halo lies within 100kpc $h^{-1}$ of the target halo in more than 90 per cent of the cases. In 76 per cent of the cases, the present virial masses differ by less than 10 per cent, while in 95 per cent of the cases matched haloes have virial masses that differ by less than 20 per cent at present.

Fig. 7 shows the mass accretion histories of two MW-like haloes as obtained from the MS-II (solid lines) and from the mini-MSII (dashed lines). As for previous figures, mass accretion histories have been constructed by connecting each halo to its main progenitor (i.e. the most massive) at each node of the tree. At mini-MSII resolution, it is not possible to follow the evolution of these haloes past $z \sim 7-9$, while the first progenitors of the MW-like haloes under consideration are identified at $z \sim 14-15$ at the resolution of the MS-II. Over the redshift range where haloes are identified in both simulations, the mass accretion histories extracted from the MS and mini-MSII are in quite good agreement. Most of the differences discussed below, should then be ascribed to the ability to follow the evolution of the parent dark matter haloes up to higher redshift in the higher resolution simulation.

[4] This search radius is a factor of $\sim 7$ smaller than the typical separation between $10^{12}\,h^{-1}\,M_{\odot}$.

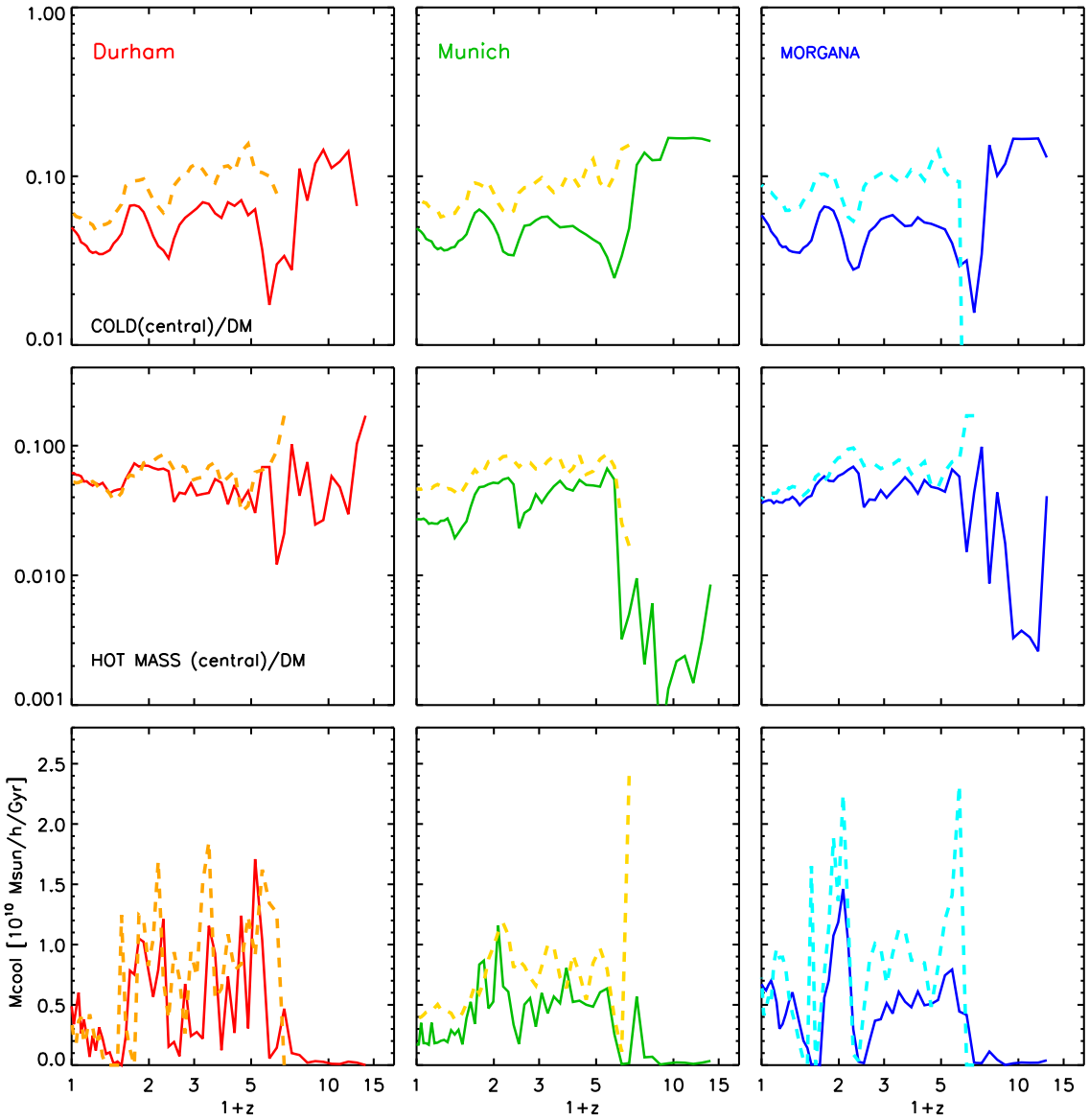


**Figure 8.** Evolution of the cold gas content (top panels), hot gas (middle panels) and the cooling rates (bottom lines) for one of the MW-like haloes used in this sample, at two different resolution levels. In each panel, solid lines show the evolution computed using the merger trees extracted from the MS-II, while dashed lines correspond to merger trees from mini-MSII. Left, middle and right panels show results from the Durham, Munich and MORGANA model, respectively. The mass accretion history of this halo is shown in the top panel of Fig. 7.

Figs. 8 and 9 show the evolution of the cold and hot gas fractions (top and middle panels respectively) and the cooling rates (bottom panels) for the two examples whose mass accretion histories are shown in Fig. 7. In these figures, solid lines show the predictions from the Durham, Munich and MORGANA models obtained using the higher resolution trees from the MS-II, while dashed lines show predictions from the lowest resolution simulations. For clarity, we have only shown the cold gas fractions obtained when merger times are set to infinity. Although the overall behaviour of cooling rates is similar in the two resolution runs, particularly at low redshift, it is clear from these figures that none of the models used in this study achieves a very good convergence. The bottom panels of Figs. 8 and 9 show that at halo appearance in the lowest resolution simulation, all three models generally predict a much larger cooling rate than obtained in the highest resolution simulation. The cooling rates adjust rapidly at approximately the levels predicted in the highest resolution simulation, but are always somewhat larger than the higher resolution predictions. As a consequence, cold gas fractions predicted using the lower resolution trees are generally higher than obtained when using the higher resolution trees.

In its standard implementation, the Munich model employed in this study, runs on subhalo-based merger trees, rather than on FOF-based trees like those that we have used in previous sections. It is then interesting to ask how much results discussed above are affected by the use of a differ-

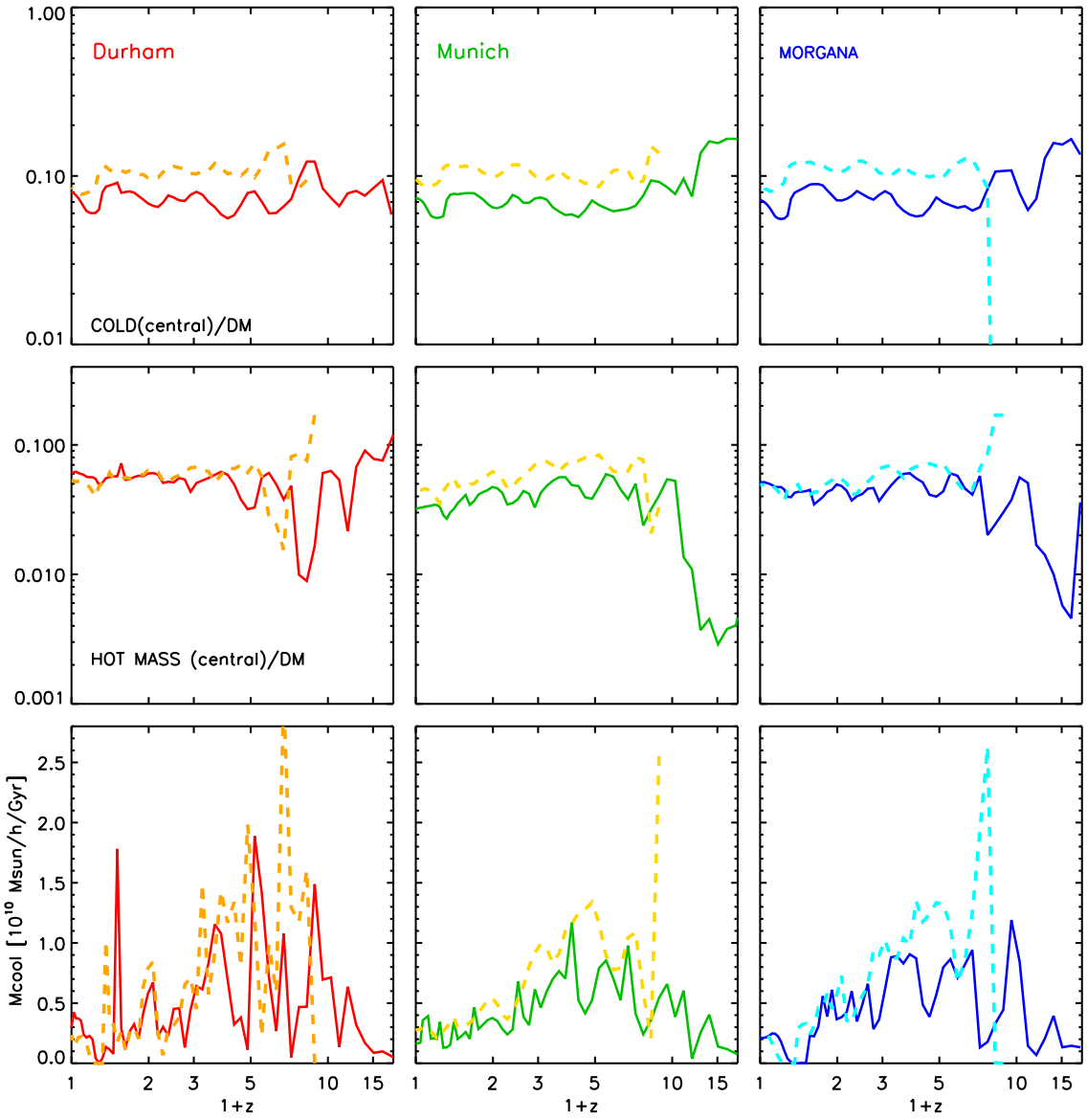


**Figure 9.** As in Fig. 8. The mass accretion history of this halo is shown in the bottom panel of Fig. 7.

ent scheme for the construction of the input merger trees. To address this question, we have run the Munich model on all the subhalo trees corresponding to the FOF trees in both the MW and SCUBA samples discussed in Section 2. We remind the reader that the subhalo-based merger trees for the MS and MS-II were constructed by Springel et al. (2005) and Boylan-Kolchin et al. (2009) as summarized in Section 2, and that they are publicly available.

Figs. 10 and 11 show the evolution of the cold gas fraction (top panels), hot gas fraction (middle panels) and cooling rates (bottom panels) of the same MW and SCUBA-like examples shown in Figs. 1 and 4. In these figures, green lines correspond to results from the FOF-based trees (and are therefore equivalent to the results from the Munich model shown in Figs. 1 and 4), while black lines show the corresponding results based on subhalo-based merger trees (red lines in Fig. 11 will be discussed in Section 8 and can be ignored for now).

These figures show that predictions obtained using the FOF-based trees are in quite nice agreement with those obtained using the subhalo-based trees. For MW-like haloes, there is some tendency for the FOF-based trees to provide lower cold and hot gas fractions with respect to results from subhalo-base trees. For the SCUBA haloes, the cold gas fractions predicted from the two schemes are very similar over all the redshift range where it is possible to trace the main progenitor of the haloes under consideration. At $z < 2$, the hot gas fraction predicted using the FOF-based trees is only slightly lower than results obtained using the standard (for the Munich model) subhalo scheme.

The bottom panels of Figs. 10 and 11 show that the cooling rates obtained using the two different schemes are very close, particularly at high redshift. Some small differ-

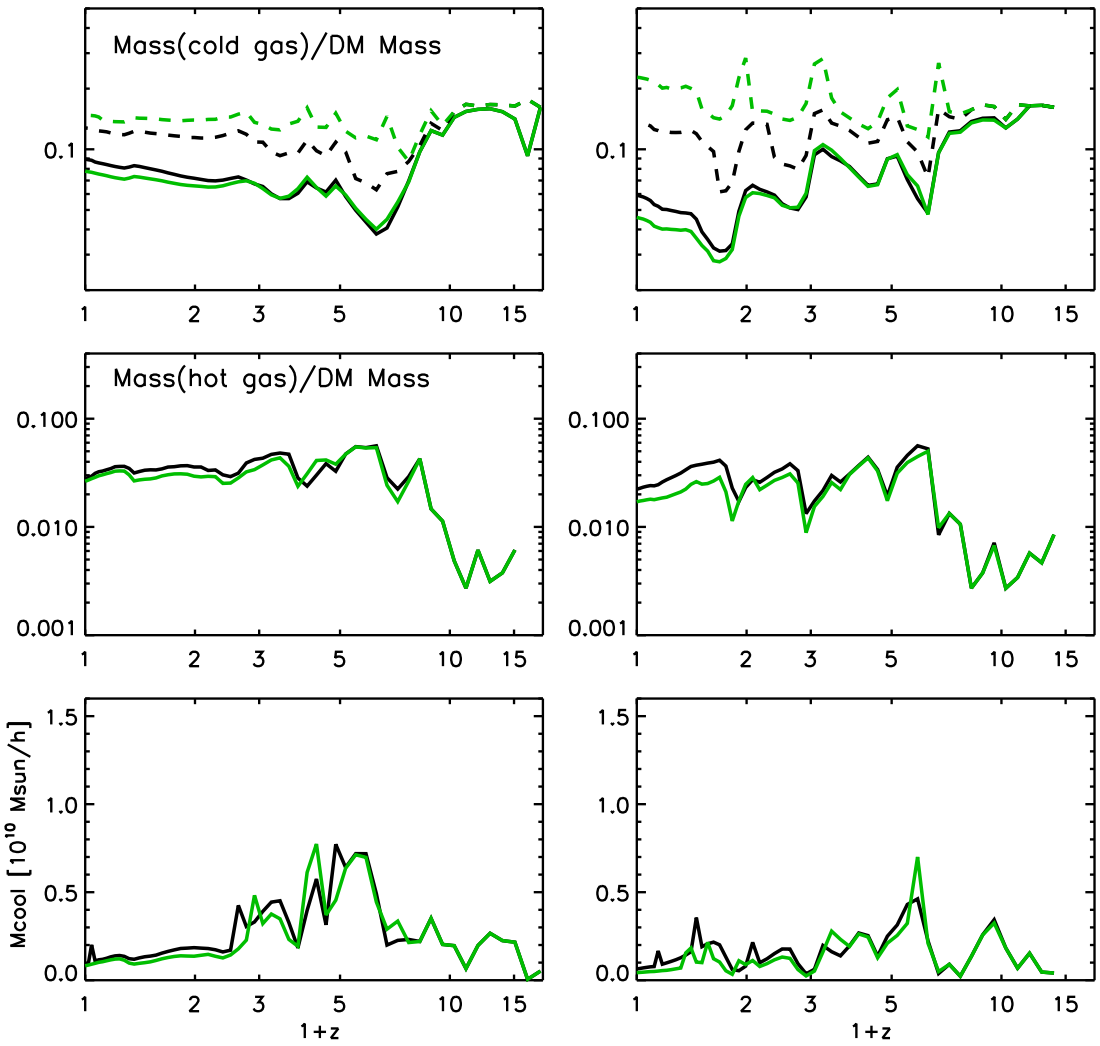


**Figure 10.** From top to bottom: cold gas fraction, hot gas fraction, and gas cooling rate for the same MW-like haloes shown in Fig. 1. Solid and dashed lines in the top panels show results for the $t_{mrg} = \infty$ and $t_{mrg} = 0$ run, respectively. Black and green lines correspond to subhalo-based and FOF-based merger trees, respectively.

ences are, however, visible. These arise from different halo merger times due to the subhalo scheme explicitly following haloes once they are accreted onto more massive systems. We recall that in the standard Munich model, a residual merging time (given by Eq. 3) is assigned to satellite galaxies only when the dark matter substructures fall below the resolution limit of the simulation. We have kept this assumption in the examples shown here so that the $t_{mrg} = 0$ case corresponds to galaxies merging at the time their parent subhaloes are tidally stripped at the resolution limit of the simulation, rather than instantaneously merging at the time their parent haloes become proper substructures. That is why the two dashed lines shown in the top panels of Figs. 10 and 11 follow a different evolution. As we have explained in Section 3, in this model the amount of gas available for cooling is computed at the beginning of each snapshot by assuming baryon conservation (see Eq. 1). Since then some cold gas is retained in distinct satellites for some time in the subhalo scheme, this leads to a different amount of gas available for cooling, and to the differences discussed above. It is interesting, however, that despite the delay due to the identification of dark matter substructures, the hot and cold gas fractions predicted by the two schemes, as well as the predicted cooling rates, do not differ dramatically. The differences between the two schemes become more important at lower redshift, but are in all cases smaller than those obtained from alternative modelling schemes (see Sections 4 and 5). This suggests that tidal stripping and truncation are very efficient in reducing the high redshift substructures below the resolution limit of the simulation, while dark matter subhaloes survive longer as independent entities at lower redshift. This is expected, due to the increase of dynamical times at later times (see also Fig. 4 in Weinmann et al. 2009).

## 7 MERGERS

In this section, we compare the different implementations of galaxy mergers adopted in the three models used in this study. To this aim, we have identified all satellites that

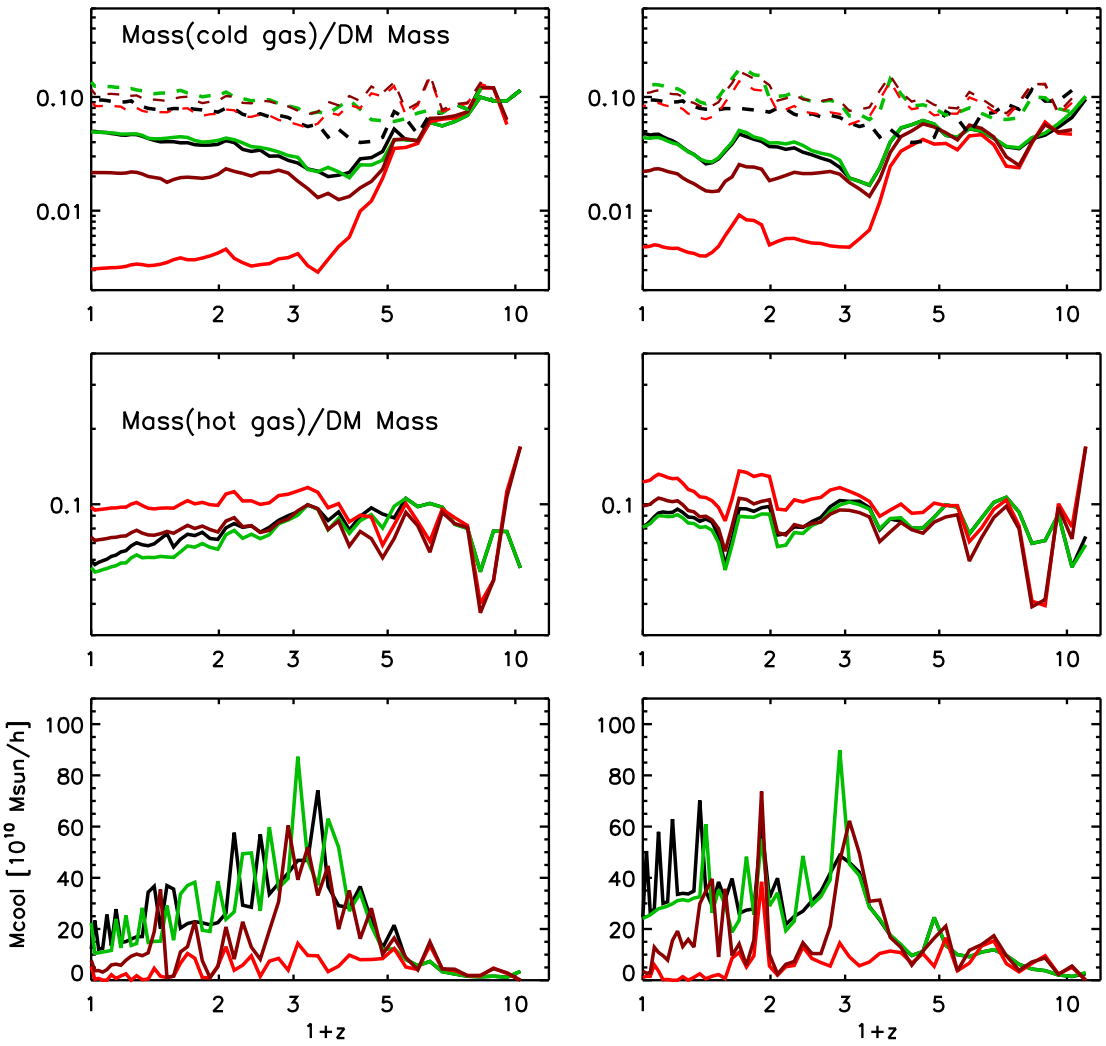


**Figure 11.** From top to bottom: cold gas fraction, hot gas fraction, and gas cooling rate for the same SCUBA haloes shown in Fig. 4. Solid and dashed lines in the top panels show results for $t_{mrg} = \infty$ and $t_{mrg} = 0$, respectively. Black and green lines correspond to subhalo based and FOF-based merger trees, while red lines correspond to the outputs from the Durham model, with darker lines showing results obtained assuming an isothermal profile for the hot gas.

are present in each pair of models[5] and that are assigned merger times that are lower than the Hubble time. As a reminder, merger times in the Durham model and in MORGANA are re-assigned after a new formation event, or halo major merger. For the comparison discussed below, we have always considered the last assignments in these two models.

Fig. 12 compares the distributions of merging times in all three models used in this study. Top panels are for satellites of the MW-like haloes, while bottom panels are for SCUBA-like haloes. There is no significant difference between the two samples, but a much larger number of satellites for the SCUBA haloes. Fig. 12 shows that a fraction of model satellites distribute along the one-to-one relation when comparing the merger times assigned in the Durham model with those obtained from the Munich model (left panels). The scatter is, however, very large, with a large number of satellites merging within relatively short times in the Munich model and getting a much longer merger time in the Durham model, and viceversa. The correlation between the Munich model and MORGANA is much tighter (middle panels in Fig. 12), but there is a clear offset indicating that model satellites in MORGANA have merger times that are systematically lower than the corresponding times from the Munich model. Finally, when comparing the Durham model and MORGANA (right panels), all satellites fall below the one-to-one relation with a quite large scatter, and there is a large concentration of galaxies that merge within $\sim 5$ Gyr in the Durham model and within $\sim 0.6$ Gyr in MORGANA.

At least part of the scatter in Fig. 12 is due to the random extraction of orbital parameters in the Durham and MORGANA models. To show a 'cleaner' comparison, we have re-run both models neglecting the orbital dependency.

[5] Due to a different treatment of the rapid cooling regime, there are haloes that host a galaxy in one model and not in another. These 'unpaired galaxies' are excluded in the analysis presented here.

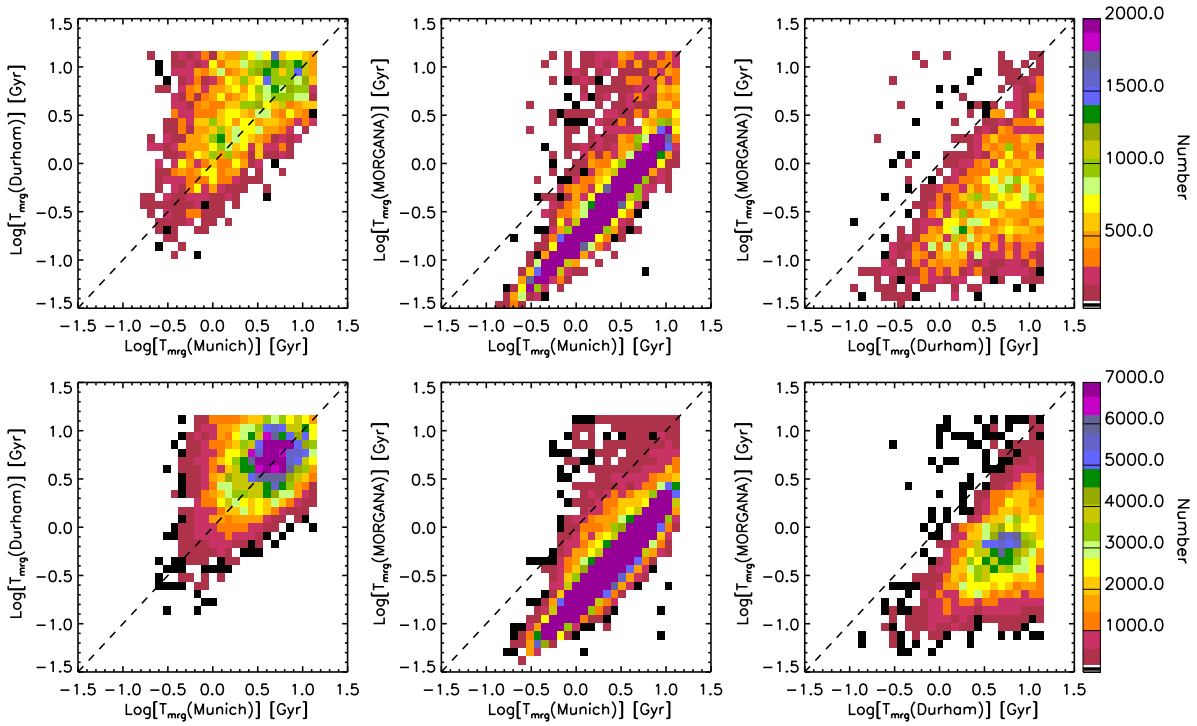


**Figure 12.** Distributions of merging times in the three models used in this study. Top panels are for MW haloes while bottom panels are for the SCUBA haloes. Maps have been computed using only satellite galaxies present in both models and with merger time smaller than the Hubble time.

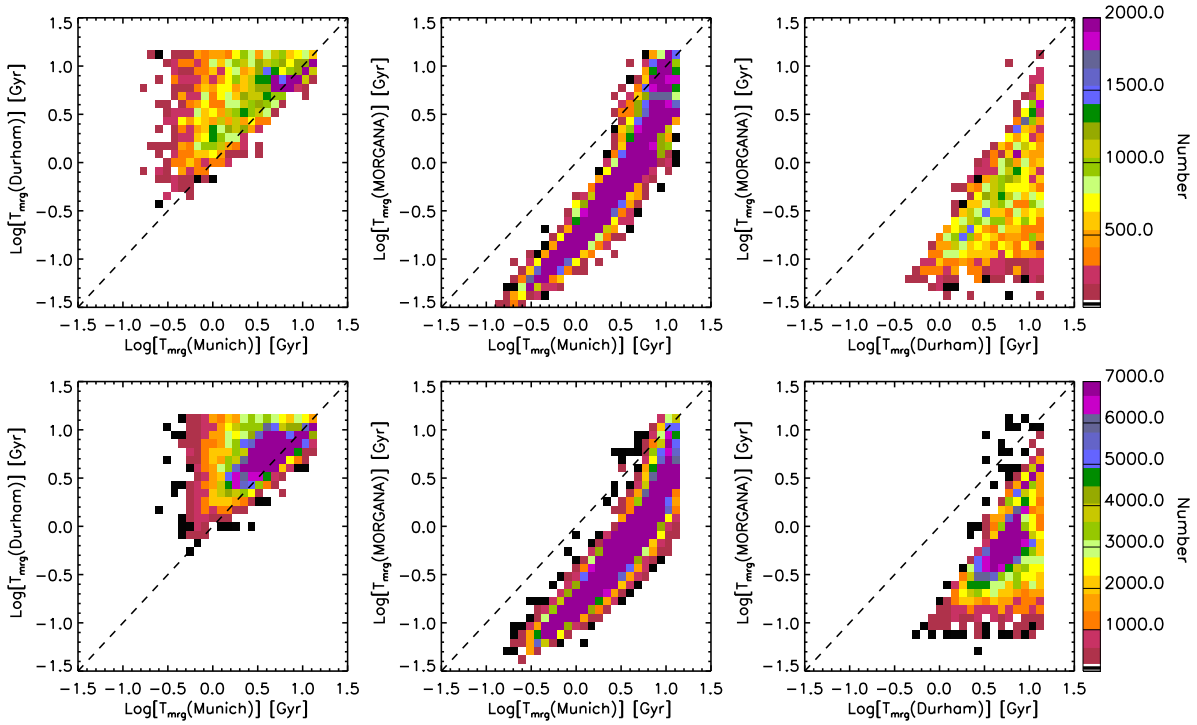


**Figure 13.** As in Fig. 12, but neglecting the orbital dependencies in the merger time calculation for the Durham and MORGANA models (see text for details).

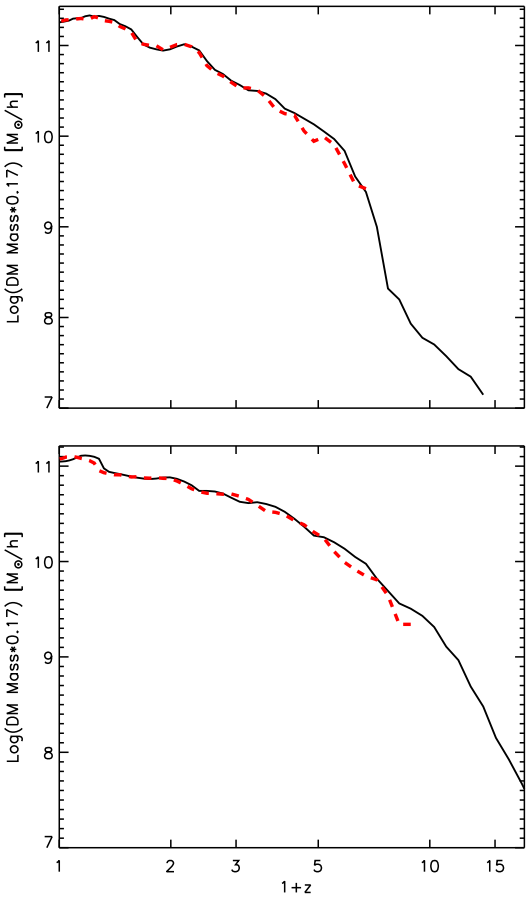


**Figure 7.** Mass accretion history of two of the haloes from the MW-like sample used in this study, at two different resolution levels. Solid lines show the histories constructed using the MS-II simulation, while dashed lines show the corresponding histories from the mini-MSII.

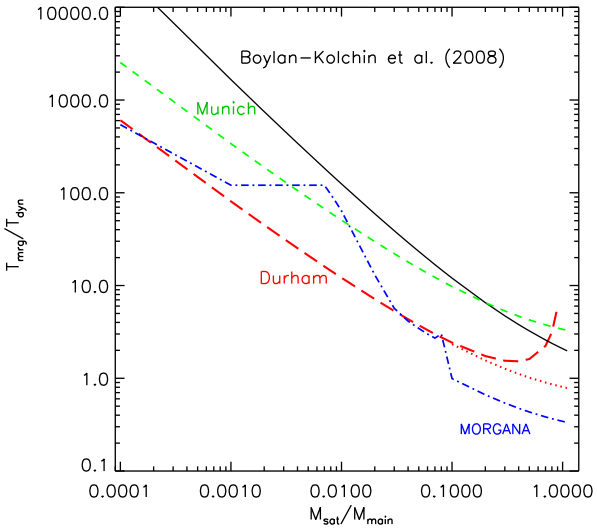


**Figure 14.** Merger times (in units of dynamical times) for different mass ratios. Dashed, long-dashed and dot-dashed lines correspond to the standard assumptions adopted by the Munich, Durham and MORGANA models respectively. The dotted line has been obtained from the long-dashed line by changing the assumption for the Coulomb logarithm to $\Lambda_{\rm df} = 1 + M_{\rm main}/M_{\rm sat}$. The predictions from MORGANA do not depend significantly on halo concentration. The thick solid line corresponds to the fitting formula provided by Boylan-Kolchin et al. (2008), with no orbital dependency and for circular orbits.

In the Durham model, this has been achieved by setting $\Theta_{\rm orbit} = 1$, while in MORGANA only circular orbits have been considered, with orbital energy set to 0.5 (see Section 3.3). Results are shown in Fig. 13. As expected, the scatter is reduced in all panels. A larger fraction of model satellites distribute along the one-to-one relation in the left panels. There is, however, still a significant fraction of satellites that get longer merger times in the Durham model than in the Munich model. As discussed in Section 3.4, the dynamical friction formulations adopted in the Munich and Durham models differ by the assumptions made for the Coulomb logarithm, and for a different numerical pre-factor. All differences visible in the left panels of Fig. 13 are due to these different assumptions, and to the re-assignment of merger times after each formation event (see below).

There is still a strong correlation between the merger times assigned in MORGANA and in the Munich model, with an offset towards lower merger times in MORGANA. Neglecting the orbital dependency, the offset reduces at long merger times. The correlation between MORGANA and the Durham model is still quite bad, with a large fraction of satellites that merge within 0.6 Gyr in MORGANA and that are assigned merger times that are about ten times longer in the Durham model.

The results discussed above can be understood by comparing Eqs. 3, 5, and 6. This is done in Fig. 14, which shows the merger times obtained using these different formulations, for different mass ratios. In this figure, we have neglected the orbital dependencies and have assumed that halo concentration (this enters the equations adopted in MORGANA) varies as a function of mass according to Eq. 4 in Neto et al. (2007). The figure shows clearly that the Munich and Durham implementations differ by a scaling factor but for $M_{\rm sat}/M_{\rm main} \geqslant 0.1$, due to a different assumption about the Coulomb logarithm: the dotted line in Fig. 14 has been obtained from the long-dashed line by changing the assumption for the Coulomb logarithm to $\Lambda_{\rm df} = 1 + M_{\rm main}/M_{\rm sat}$, as in the Munich model. The re-calculation of merger times after each formation event or major merger apparently does not affect significantly the expected disagreement. It should be noted that in Figs. 12 and 13, we have only used satellite galaxies with merger times lower than the Hubble times. These figures are therefore dominated by mergers with $M_{\rm sat}/M_{\rm main} \geqslant 0.1$. In this regime, the MORGANA model is offset low with respect to the Munich model. It also predicts systematically lower merger times with respect to the Durham model but in this case the offset is not linear as a function of the mass ratio. In Fig. 14, we have also shown the fitting formula provided by Boylan-Kolchin et al. (2008), with no orbital dependency and for circular orbits. As noted earlier, the adoption of a simple fudge factor does not suffice to bring the formulation adopted in the Munich

model in agreement with the new fitting formula proposed by Boylan-Kolchin et al.

## 8 SUMMARY AND DISCUSSION

In this work we have compared results from three independently developed semi-analytic models, and we have focused on alternative implementations of gas cooling and galaxy mergers. Our model comparison is carried out using two large samples of *identical* merger trees, which allows us to compare results on a case-by-case basis and to focus on differences due to different model assumptions and parametrizations. In particular, we have constructed two FOF-based merger tree samples. One is a set of 100 haloes from the MS-II with redshift zero dark matter halo masses similar to that of the Milky Way (MW-like haloes), while the other consists of 100 haloes from the MS with a number density similar to that measured for SCUBA galaxies at $z \sim 2$ (SCUBA-like haloes). By using stripped-down versions of the models, we are able to avoid possible degeneracies and complications due to a different treatment of various physical processes and to concentrate on the influence of specific assumptions and/or parametrizations. As explained above, we have chosen to include only the processes of gas cooling and galaxy mergers. In the following, we summarize briefly the results obtained and discuss them.

### 8.1 Gas cooling

Our results show that the different assumptions adopted about gas cooling lead to very similar results on mass scales similar to those of our own Galaxy, and to a generally good statistical agreement. Important differences arise, however, on larger mass scales.

Two of the models used in this study (the Munich and Durham models) assume variations of the cooling model originally proposed by White & Frenk (1991). The other model used here (MORGANA) adopts a more sophisticated model and, on the basis of previous published results (Viola et al. 2008), was expected to provide systematically higher cooling rates for our SCUBA-like haloes. Contrary to this naive expectation, however, results from the Munich model and from MORGANA are very similar for this mass scale, while the Durham model gives systematically lower cooling rates. These results appear to be in contradiction with previously published tests, but the contradiction is only apparent as we discuss below.

As explained in detail in Section 3, although the Munich and Durham models are variations of the same cooling model, they differ in a number of details, in particular for the assumption adopted for the hot gas distribution. Red lines in Fig. 11 show results from the standard Durham model (that assumes a $\beta$ profile for the hot gas) and from a model that uses the same cooling implementation but assumes an isothermal distribution for the hot gas (darker red lines), as in the Munich model. The figure shows clearly that by changing this assumption, the predicted cooling rates are larger, bringing model results closer to (although they are still lower than) those obtained from the Munich model (green lines in Fig. 11). Some differences are still apparent, however: the Munich model predicts systematically higher cooling rates than the Durham model, particularly at high redshift, where cooling is much more efficient in this model than in both of the Durham implementations considered here. These residual differences are due to a number of other different assumptions, in particular for the calculation of the cooling radius (see Section 3.4). Statistically, the differences between the models are relatively *small*, which reflects a general agreement in the underlying framework of these two models.

Perhaps more surprising is the similarity between the results obtained from the Munich model and those from MORGANA, at both mass scales analysed in this paper. As discussed earlier, Viola et al. (2008) have claimed that the cooling model implemented in MORGANA predicts cooling rates that are significantly larger than those obtained using the classical model by White & Frenk (1991). It should be noted, however, that their implementation of the classical model did not assume any special treatment for the 'rapid cooling regime' (as is instead done in the original work by White and Frenk and all subsequent variants of this model), and assumed that the hot gas distribution is described by a polytropic equation of state with index $\gamma_p = 1.15$, which is similar to the $\beta$ profile assumed in the Durham model. In addition, results discussed in Viola et al. were obtained for isolated static haloes and it is not trivial to generalize them to the case of cosmological mass accretion histories, like those we have used here. Their conclusions is, however, valid when one adopts a gas distribution similar to that adopted in the Durham model used in this study (which is indeed similar to that they assumed in their implementation of the classical model). Adopting a steeper gas profile, as in the Munich model used here, changes results significantly in some mass regimes, bringing them in very good agreement with those from the MORGANA model.

It is important to realize that the differences highlighted above will have important consequences on predictions from galaxy formation models. For example, the Munich and MORGANA models will need to assume a stronger feedback than the Durham model, to counter-act excessive cooling at low redshift in relatively large haloes. Although all models achieve this using very similar schemes (the AGN feedback), the relative importance of these additional physical processes will be different in these three models. Predicting much lower cooling rates for massive haloes, the Durham model will have difficulties in providing large numbers of galaxies with elevated star formation at high redshift. Indeed, this model is able to reproduce the observed galaxy number counts at 850$\mu$m only by assuming a top-heavy initial mass function (IMF) from the stars formed in bursts. This works because a top-heavy IMF has a much larger recycled gas fraction, which provides fuel for star formation. As illustrated above, MORGANA predicts much larger cooling rates than the Durham model and is indeed able to reproduce the number counts of submillimiter sources (but the brightest ones) with a standard IMF (Fontanot et al. 2007). The Munich model used in this study predicts even larger cooling rates on average, but its predictions for the submillimiter number counts have not been explored yet.

### 8.2 Galaxy mergers

The three models used in this study adopt a different modelling for galaxy mergers. The Munich and Durham model assume variations of the classical dynamical friction formula. Results from these two models are somewhat correlated, but there is a large scatter and a large number of galaxies get significantly longer merger times in one model than in the other. As explained in Section 7, this is mainly due to the adoption of a different numerical factor in front of the dynamical friction formula employed, and to a different assumption about the Coulomb logarithm. MORGANA uses formulae derived from numerical simulations and analytic models that take into account dynamical friction, mass loss by tidal stripping, tidal disruption of subhaloes, and tidal shocks (Taffoni et al. 2003). As shown above, over the range of mass-ratios that provide merger times lower than the Hubble time, the merger times obtained using these formulae are systematically lower (by a factor $\sim 10\,\tau_{\rm dyn}$) than those computed from the Munich model. Of the three models used in this study, the Munich model uses merger times that are closer to the fitting formula recently proposed by Boylan-Kolchin et al. (2008), when neglecting any orbital dependence.

The differences just discussed have important consequences for the stellar assembly history of massive galaxies, and for the formation and evolution of the brightest cluster galaxies and of the intra-group and intra-cluster light. MORGANA (and to some extent also the Durham model) will tend to assemble massive central galaxies earlier than the Munich model. To keep these galaxies red, these models will need to assume a somewhat stronger supernovae feedback so as to make most of the mergers driving their late stellar assemble *dry* (i.e. avoid triggering late bursts that would rejuvenate the stellar population of these galaxies). A different balance between AGN cooling and tidal stripping of stars will also be required in these models to keep model predictions in agreement with observational results. These considerations are of course valid in the case all models would use the same treatment of all other physical processes at play. We remind, however, that as mentioned in Section 1, these processes are usually treated in a different way complicating the comparison between different models.

### 8.3 Numerical resolution and merger tree scheme

Taking advantage of the mini-MSII, run using the same initial conditions and volume as for the MS-II but lower resolutions, we have analysed how the results discussed above vary as a function of numerical resolution. The level of agreement between the three models used in our study is not affected by numerical resolution. None of the models used in this paper, however, achieves a good numerical convergence, with all of them predicting moderately larger cooling rates in lower resolution runs.

On the other hand, results seem to be quite stable to alternative schemes for the construction of dark matter merger trees. In particular, we have compared results obtained using FOF-based trees with those obtained using subhalo-based trees, which represent the standard input of the Munich model used in this study. The small differences found by comparing results from these two schemes can be ascribed to the possibility of tracking the accreted haloes until they are stripped below the resolution limit of the simulation by tidal stripping and truncation. Interestingly, our results show that these processes act on relatively short time-scales, and that they are more efficient at higher redshift.

### 8.4 What Next?

One question that this study does not address is: what is the *best* way to model gas cooling and galaxy mergers? This is a very difficult question, particularly for the cooling model. It is clear that one needs to understand how the gas is distributed in dark matter haloes, and how this distribution is affected by heating from supernovae and/or AGN feedback. Although hydrodynamical simulations of galaxy formation are becoming increasingly sophisticated, these physical processes still need to be included as 'sub-grid' physics, i.e. using prescriptions that are 'semi-analytical' in nature. As a consequence, published hydrodynamical simulations offer little indication of appropriate modelling of the hot gas distribution and evolution.

Our results have pointed out that modelling of the rapid cooling regime differ significantly in the implementations discussed in this paper. Substantial numerical work has been focused recently on this mode of accretion, although it was was discussed as early as Binney (1977), Rees & Ostriker (1977), and White & Frenk (1991). Interestingly, recent studies show that gas accretion during the 'quasi-static regime' in hydrodynamical simulations is sensitive to different implementations of SPH (Kereš et al. 2009, see also Yoshida et al. 2002), while accretion rates in the rapid cooling regime are quite robust. One possible additional concern in using numerical results to inform semi-analytic models is the poor performance of SPH codes in resolving and treating dynamical instabilities developing at sharp interfaces in a multi-phase fluid (Agertz et al. 2007).

The situation is somewhat better for the modelling of galaxy mergers. Since the merging process is predominantly driven by gravity, it can be studied using controlled numerical experiments as done, for example, by Boylan-Kolchin et al. (2008). As noted earlier, however, recent work has not yet converged on the dynamical friction formula appropriate for galaxy formation models. Further work in this area is therefore needed.

Gas cooling and galaxy mergers are two basic ingredients of any galaxy formation model that are relatively well understood. Also at this level, however, different assumptions have to be made when implementing these processes. These give rise to non-negligible differences that can have important implications on the weight that needs to be given to additional physical processes (e.g. AGN feedback, tidal stripping of stars, etc.). This paper highlights specific areas where further work is needed in order to improve our galaxy formation models, with the ultimate goal of improving our understanding of the physical processes driving galaxy formation and evolution.

## ACKNOWLEDGEMENTS

GDL acknowledges financial support from the European Research Council under the European Community's Seventh

Framework Programme (FP7/2007-2013)/ERC grant agreement n. 202781. AJB acknowledges the support of the Gordon & Betty Moore Foundation. GDL, AJB, and FF acknowledge the hospitality of the Kavli Institute for Theoretical Physics of Santa Barbara, where the initial calculations that led to this paper were carried out. The Millennium and Millennium-II Simulation databases used in this paper and the web application providing online access to them were constructed as part of the activities of the German Astrophysical Virtual Observatory. We are grateful to Gerard Lemson for setting up an internal database that greatly facilitated the exchange of data and information needed to carry out this project. We are grateful to Carlton Baugh, Richard Bower, Shaun Cole, Carlos Frenk and Cedric Lacey for making available the Galform code for this project.

This paper has been typeset from a TEX/ LATEX file prepared by the author.

## REFERENCES

Agertz O., Moore B., Stadel J., Potter D., Miniati F., Read J., Mayer L., Gawryszczak A., Kravtsov A., Nordlund Å., Pearce F., Quilis V., Rudd D., Springel V., Stone J., Tasker E., Teyssier R., Wadsley J., Walder R., 2007, MNRAS, 380, 963

Baugh C. M., 2006, Reports of Progress in Physics, 69, 3101

Benson A. J., Bower R. G., Frenk C. S., Lacey C. G., Baugh C. M., Cole S., 2003, ApJ, 599, 38

Benson A. J., Kamionkowski M., Hassani S. H., 2005, MNRAS, 357, 847

Benson A. J., Pearce F. R., Frenk C. S., Baugh C. M., Jenkins A., 2001, MNRAS, 320, 261

Binney J., 1977, ApJ, 215, 483

Bond J. R., Cole S., Efstathiou G., Kaiser N., 1991, ApJ, 379, 440

Bower R. G., 1991, MNRAS, 248, 332

Bower R. G., Benson A. J., Malbon R., Helly J. C., Frenk C. S., Baugh C. M., Cole S., Lacey C. G., 2006, MNRAS, 370, 645

Boylan-Kolchin M., Ma C.-P., Quataert E., 2008, MNRAS, 383, 93

Boylan-Kolchin M., Springel V., White S. D. M., Jenkins A., 2010, arXiv:0911.4484 [astro-ph]

Boylan-Kolchin M., Springel V., White S. D. M., Jenkins A., Lemson G., 2009, MNRAS, 398, 1150

Cattaneo A., Blaizot J., Weinberg D. H., Kereš D., Colombi S., Davé R., Devriendt J., Guiderdoni B., Katz N., 2007, MNRAS, 377, 63

Chapman S. C., Smail I., Blain A. W., Ivison R. J., 2004, ApJ, 614, 671

Cole S., 1991, ApJ, 367, 45

Cole S., Helly J., Frenk C. S., Parkinson H., 2008, MNRAS, 383, 546

Cole S., Lacey C., 1996, MNRAS, 281, 716

Cole S., Lacey C. G., Baugh C. M., Frenk C. S., 2000, MNRAS, 319, 168

De Lucia G., Blaizot J., 2007, MNRAS, 375, 2

De Lucia G., Kauffmann G., Springel V., White S. D. M., Lanzoni B., Stoehr F., Tormen G., Yoshida N., 2004, MNRAS, 348, 333

De Lucia G., Kauffmann G., White S. D. M., 2004, MNRAS, 349, 1101

Fakhouri O., Ma C., 2008, MNRAS, 386, 577

Ferland G. J., Korista K. T., Verner D. A., Ferguson J. W., Kingdon J. B., Verner E. M., 1998, PASP, 110, 761

Fontanot F., Monaco P., Silva L., Grazian A., 2007, MNRAS, 382, 903

Genel S., Genzel R., Bouché N., Sternberg A., Naab T., Schreiber N. M. F., Shapiro K. L., Tacconi L. J., Lutz D., Cresci G., Buschkamp P., Davies R. I., Hicks E. K. S., 2008, ApJ, 688, 789

Helly J. C., Cole S., Frenk C. S., Baugh C. M., Benson A., Lacey C., Pearce F. R., 2003, MNRAS, 338, 913

Jiang C. Y., Jing Y. P., Faltenbacher A., Lin W. P., Li C., 2008, ApJ, 675, 1095

Kauffmann G., White S. D. M., Guiderdoni B., 1993, MNRAS, 264, 201

Kereš D., Katz N., Fardal M., Davé R., Weinberg D. H., 2009, MNRAS, 395, 160

Li Y., Mo H. J., van den Bosch F. C., Lin W. P., 2007, MNRAS, 379, 689

Monaco P., Fontanot F., Taffoni G., 2007, MNRAS, 375, 1189

Monaco P., Theuns T., Taffoni G., Governato F., Quinn T., Stadel J., 2002, ApJ, 564, 8

Neto A. F., Gao L., Bett P., Cole S., Navarro J. F., Frenk C. S., White S. D. M., Springel V., Jenkins A., 2007, MNRAS, 381, 1450

Rees M. J., Ostriker J. P., 1977, MNRAS, 179, 541

Saro A., De Lucia G., Borgani S., Dolag K., 2010, arXiv:1001.3115

Springel V., White S. D. M., Jenkins A., Frenk C. S., Yoshida N., Gao L., Navarro J., Thacker R., Croton D., Helly J., Peacock J. A., Cole S., Thomas P., Couchman H., Evrard A., Colberg J., Pearce F., 2005, Nature, 435, 629

Springel V., White S. D. M., Tormen G., Kauffmann G., 2001, MNRAS, 328, 726

Sutherland R. S., Dopita M. A., 1993, ApJS, 88, 253

Taffoni G., Mayer L., Colpi M., Governato F., 2003, MNRAS, 341, 434

Viola M., Monaco P., Borgani S., Murante G., Tornatore L., 2008, MNRAS, 383, 777

Weinmann S. M., Kauffmann G., von der Linden A., De Lucia G., 2009, ArXiv:0912.2741

White S. D. M., Frenk C. S., 1991, ApJ, 379, 52

White S. D. M., Rees M. J., 1978, MNRAS, 183, 341

Yoshida N., Stoehr F., Springel V., White S. D. M., 2002, MNRAS, 335, 762